Changing sources and burial of organic carbon in the Chukchi Sea sediments with retreating sea ice over recent centuries

Liang Su[1,2], Jian Ren[2*], Marie-Alexandrine Sicre[3], Youcheng Bai[2], Ruoshi Zhao[1,2], Xibing Han[4], Zhongqiao Li[2], Haiyan Jin[2,5], Anatolii S. Astakhov[6], Xuefa Shi[7], Jianfang Chen[2,5*]

[1] Ocean College, Zhejiang University, Zhoushan 316021, China

[2] Key Laboratory of Marine Ecosystem Dynamics, Second Institute of Oceanography, Ministry of Natural Resources, Hangzhou 310012, China

[3] Sorbonne Université, Pierre et Marie Curie, CNRS, LOCEAN, Case 100, 4 Place Jussieu, F-75005 Paris, France

[4] Key Laboratory of Submarine Geosciences, Second Institute of Oceanography, Ministry of Natural Resources, Hangzhou 310012, China

[5] State Key Laboratory of Satellite Ocean Environment Dynamics, Second Institute of Oceanography, Ministry of Natural Resources, Hangzhou 310012, China

[6] V.I. Il'ichev Pacific Oceanological Institute, Far Eastern Branch of Russian Academy of Sciences, Vladivostok 690041, Russia

[7] Key Laboratory of Marine Geology and Metallogeny, First Institute of Oceanography, Ministry of Natural Resources, Qingdao 266061, China

Correspondence to: Jian Ren (jian.ren@sio.org.cn) and Jianfang Chen (jfchen@sio.org.cn)

Abstract. Decreasing sea ice extent caused by climate change is affecting the carbon cycle of the Arctic Ocean. In this study, surface sediments across the western Arctic Ocean are investigated to characterize sources of sedimentary organic carbon (OC). Bulk organic parameters (total organic carbon, total nitrogen, $\delta^{13}C_{org}$ and $\delta^{15}N$) and molecular organic biomarkers (e.g., sterols and highly branched isoprenoids (HBIs)) are combined to distinguish between sympagic, pelagic, and terrestrial OC sources. Their downcore profiles generated at the Chukchi Sea R1 core site (74 °N) are then used to evaluate changes in the relative contribution of these components of sedimentary OC over the last 200 years with decreasing sea ice. Our data evidence that from 1820s to 1930s prevailing high sea ice cover inhibited *in situ* primary production resulting in prominent land-derived material in sediments. Then, from 1930s to 1980s, primary production starts increasing with the gradual decline of summer sea ice. The ratio of sympagic and pelagic OC began to rise to account for the larger portion of sedimentary OC. Since 1980s, accelerated sea ice loss led to enhanced primary production, stabilizing over the last decades due to freshwater induced surface ocean stratification in summer.

1 Introduction

Knowledge on processes and feedback mechanisms controlling the carbon cycle is essential for a better understanding of Arctic marine ecosystem dynamics and its role in climate change (Parmentier et al., 2017; Wheeler et al., 1996). The Arctic Ocean is the major world carbon sink region where huge amounts of marine and terrestrial organic carbon (OC) have accumulated (Stein et al., 2004). Today, the Arctic Ocean experiences unprecedented changes caused by global warming and Arctic amplification (Cavalieri et al., 1997; Rantanen et al., 2022; Serreze and Francis, 2006; Shindell and Faluvegi, 2009) which have resulted in major sea ice loss with consequences on the marine ecosystems and Arctic carbon budget. Increased river discharge and melting permafrost are responsible for enhanced delivery of terrigenous inorganic and organic carbon to the Arctic marginal seas (Grotheer et al., 2020; Holmes et al., 2011; Rawlins et al., 2021; Vonk et al., 2012). Terrigenous OC reaching the Arctic Ocean is either partly mineralized or transported to the sea floor where it is ultimately buried (Fritz et al., 2017; Tanski et al., 2019). Increased nutrient-rich waters brought by enhanced Pacific water inflow (PWI), a major source of nutrients to the Arctic, also contribute to stimulate phytoplankton productivity in the western Arctic Ocean (Arrigo and van Dijken, 2015; Tian et al., 2021; Woodgate and Peralta-Ferriz, 2021; Woodgate, 2018). Lastly and most importantly, the rapid sea ice loss in summer has resulted in large areas of the Arctic Ocean that shifted from multi-years to seasonal sea ice coverage (Cavalieri and Parkinson, 2012; Parkinson et al., 1999; Stroeve et al., 2007) allowing higher light penetration in surface waters thereby enhancing primary production and export of OC to the bottom floor. Enhanced summer sea ice melting further contributes to sea ice algal production, export and burial of marine OC in sediments (Ardyna and Arrigo, 2020). The Chukchi Sea (CS) is one of the most productive regions of the Arctic marginal seas (Cai et al., 2010; Ouyang et al., 2022; Zhuang et al., 2022). With the rapid sea ice retreat, the CS has become a key area to study climate induced OC changes since the beginning of the Industrial Era.

A large variety of indicators, including bulk geochemical ratios and lipid biomarkers (Volkman, 1986) have been developed to characterize the composition of OC in Arctic Ocean sediments (Fernandes and Sicre, 2000; Sparkes et al., 2015). Among them, lignins and $\delta^{13}C_{org}$ have been successfully used to provide reliable estimates of terrestrial OC (Tesi et al., 2014; Wang et al., 2019a; Wild et al., 2022).

However, pelagic and sympagic sourced OC remains difficult to discriminate in the Arctic Ocean, particularly in regions of high sympagic productivity. To address this issue, the H-print index based on highly-branched isoprenoids (HBIs) defined as the ratio of pelagic HBI-III over the sum of HIBs (IP_{25} + HBI-II + HBI-III) was developed (Brown et al., 2014b; Koch et al., 2020). Values close to 100% are thus indicative of prominent pelagic sources while those close to 0% reflect prevailing sympagic sources. By combining H-print and $\delta^{13}C_{org}$, we here intend to more accurately quantify marine pelagic, marine sympagic and terrestrial fractions of OC in Arctic sediments.

Documenting changes in sea ice changes and induced transformations of Arctic ecosystems is key to better predict how the carbon cycle will respond to future changes with continued warming (Arrigo et al., 2008; Bates and Mathis 2009). Extensive surveys of Arctic sea ice have been possible only since the 1970s with the development of remote sensing observations (Cavalieri et al., 1996). Prior to this, very few *in situ* observations on sea ice exists due to the inaccessibility of the Arctic Ocean. Paleoclimate proxies such as fossils assemblages and geochemical indicators have thus been used as alternative approaches to document past changes of sea ice and place them in the context of ongoing changes (e.g. Belt, 2018; de Vernal et al., 2013 and references therein). The monounsaturated HBI biomarker IP_{25} (Ice Proxy with 25 carbon atoms) produced by sea ice diatoms was initially proposed to assess seasonal sea ice cover (Belt et al., 2007; Massé et al., 2008). The PIP_{25} (Phytoplankton-IP_{25}) index, that combines IP_{25} with pelagic phytoplankton biomarkers, was then proposed to provide semi-quantitative estimates of seasonal sea ice (Belt, 2019; Müller et al., 2011). Most IP_{25}-related studies in the Arctic Ocean have focused on surface sediments to derive spatial seasonal sea ice distribution (Kolling et al., 2020; Stoynova et al., 2013; Su et al., 2022; Xiao et al., 2015a; Xiao et al., 2013). Others have investigated its past variability at the millennial scale and beyond (Cronin et al., 2013; Polyak et al., 2016; Stein et al., 2017; Xiao et al., 2015b), but only a limited number has explored sea ice variability over the past centuries (Bai et al., 2022; Hu et al., 2020; Kim et al., 2019). None have attempted to link seasonal sea ice changes to sedimentary OC composition since the beginning of the Industrial Era.

In this study, we investigate the potential of H-print combined with $\delta^{13}C_{org}$ in surface sediments of the northern CS to discriminate and quantify the relative contribution of OC originating from pelagic, sympagic and terrestrial sources and their evolution over the last two centuries under changing sea ice

conditions to improve our understanding of ongoing alteration of the OC cycle.
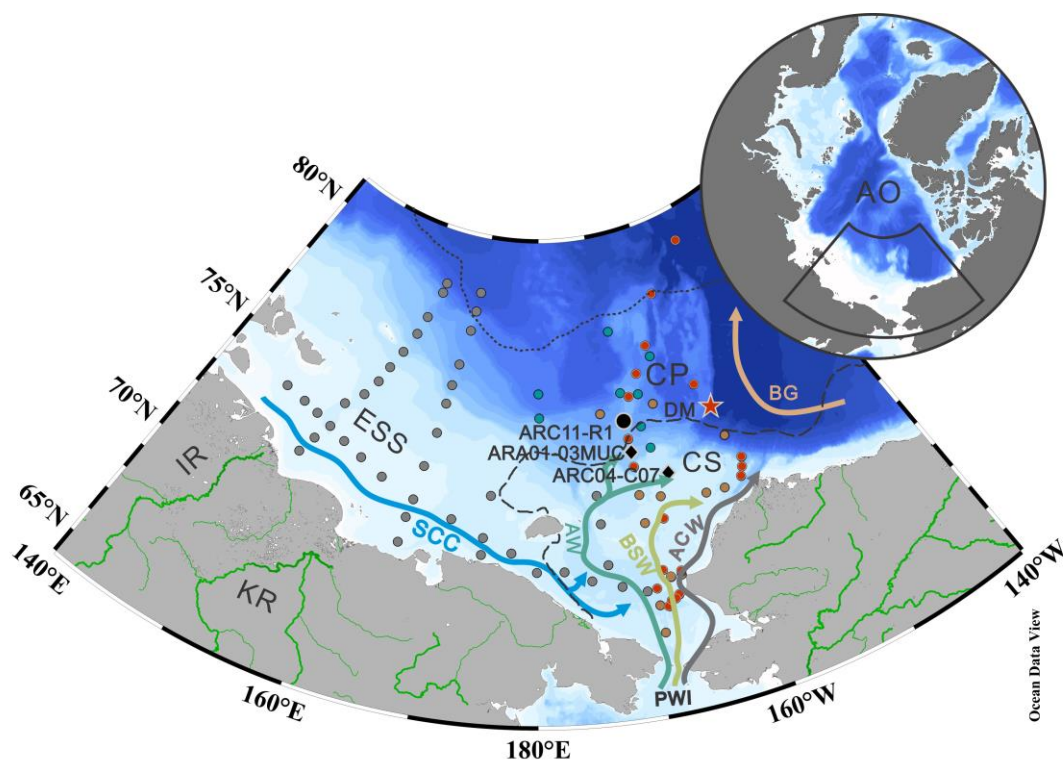
Figure 1. Map of the western Arctic Ocean (AO) showing surface ocean circulation and sampling locations (black, gray, and green dots). The stations in gray and green represent the surface samples collected on the LV77 and 11th CHINARE cruises, respectively. The black dot indicates the sediment core ARC11-R1 location. The black diamonds show two other sediment cores discussed in the text (ARC04-C07, Bai et al 2022; ARA01-03MUC, Kim et al 2019). Surface sediments reported by Bai et al. (2019) and Wang et al. (2017) are shown by red and orange dots, respectively. The red start shows the location of the sediment trap station DM (Bai et al., 2019). The dotted and dashed lines in black represent the 20% isolines of September sea ice concentration for the 2019 and 1979, respectively (https://nsidc.org; Cavalieri et al., 1996). Main study regions: ESS, East Siberian Sea; CS, Chukchi Sea; CP, Chukchi Plateau. Main surface currents: SCC, Siberian coastal current; PWI, Pacific water inflow; ACW-Alaskan Coastal Water; AW-Anadyr Water; BSW-Bering Shelf Water. Rivers are shown in green lines: IR, Indigirka River; KR, Kolyma River.

2 Oceanographic setting

The CS is one of the largest marginal seas in the world located on the northern Asian and American continents (Jakobsson, 2002). The surface ocean circulation in the CS is controlled by winds and sea ice cover (Ovall et al., 2021). This basin is connected to the Pacific Ocean through the Bering Strait. The PWI entering the Arctic Ocean strongly influences the physico-chemical water properties of the Arctic Ocean and contributes to enhanced primary production (Coachman and Aagaard, 1966) (Fig. 1). In the CS, the PWI divides into three branches: the highly saline and high-nutrient content Anadyr Water (AW)

on the western side, the fresher and oligotrophic Alaska Coastal Water (ACW) on the eastern side, and

the moderately saline Bering Shelf Water (BSW) in between (Grebmeier et al., 2006; Hunt et al., 2013;

Woodgate et al., 2005). The eastern side of the CS is adjacent to the Beaufort Sea. The dynamics of the

Beaufort Gyre (BG) also impacts on the characteristics of the CS water mass (Timmermans and Toole,

115   2023). In particular, enhanced anticyclonic BG circulation has resulted in increased freshwater

convergence into the Canadian Basin in recent years (Giles et al., 2012) with implications on the local

biological production as well as on the transport of terrestrial organic matter (He et al., 2012; Coupel et

al., 2015; Ren et al., 2020). Fresh and cold waters from the seasonal Siberian coastal current (SCC) is

another feature of the surface ocean circulation that lowers salinity of the central CS water (Weingartner

120   et al., 1999). The dramatic loss of sea ice in summer caused by global warming is particularly tangible

in the Arctic Ocean marginal seas (Cavalieri et al., 1997; Parkinson et al., 1999; Polyakov et al., 2003;

Zhang et al., 2021) and most pronounced in the CS both in terms of sea ice extent and thickness (Serreze

and Stroeve 2015; Wang et al., 2019b). Remote sensing data (1979 to 2020) reveal considerable seasonal

variations of sea ice extent in the CS. The CS is heavily covered by sea ice from November to June. Sea

125   ice gradually decreases in July and reaches its minimum extent in September (https://nsidc.org; Cavalieri

et al., 1996).

3 Material and methods

3.1 Material

A total of 42 surface sediments (0-2 cm) from the East Siberian Sea (ESS) and CS were collected

130   during the Cruise LV77 on board the R/V *Akademik M.A. Lavrentiev*. Additional 11 surface sediments

(0-2 cm) and a 15 cm long sediment core ARC11-R1 (R1 hereafter, 74.64 °N, 169.13 °W, 200 m water

depth) were also collected using a box corer and a multi-corer, respectively, in the CS and Chukchi

Plateau (CP) during the 11th Chinese National Arctic Research Expedition (CHINARE) in summer 2020

on board the R/V *Xuelong 2* (Fig. 1). Subsampling was performed on board at a sampling interval of 1

135   cm. Subsampled core sediments and surface sediments were frozen immediately after recovery at -20 °C

until further analysis in the laboratory.

3.2 Sediment core chronology

The chronology of the R1 core is based on excess ^{210}Pb (^{210}Pb$_{ex}$) determinations performed at the

State Key Laboratory of Estuarine and Coastal Research, East China Normal University, Shanghai, China,

140   using an HPGe gamma spectrometry (GSW275L, Canberra). The $^{210}Pb_{ex}$ activity was calculated by

subtracting the supporting fraction (^{226}Ra) from the total ^{210}Pb ($^{210}Pb_{total}$) activity in the sediment. The

error in $^{210}Pb_{ex}$ is computed by propagating the error in the corresponding measured pair (^{210}Pb and ^{226}Ra).

A mean linear sedimentation rate (cm yr^{-1}) was calculated from the $^{210}Pb_{ex}$ profile using a Constant Flux-

Constant Sedimentation Rate (CF-CS) model, assuming continuous homogeneous deposition of non-

145   equilibrium ^{210}Pb in the sediment (Nittrouer et al., 1984). As ^{137}Cs was also measured during the same

gamma counting session, this radionucleide was also used to test the chronology.

3.3 Bulk analyses

Total organic carbon (TOC), total nitrogen (TN), $\delta^{13}C_{org}$, and $\delta^{15}N$ of the 42 surface sediments from

the ESS and western CS during the LV77 cruise as well as the 11 surface sediments and the R1 core

150   retrieved from the CS during the CHINARE cruise were analyzed at the Key Laboratory of Marine

Ecosystem Dynamics, Second Institute of Oceanography, Ministry of Natural Resources (MED, SIO,

MNR, Hangzhou, China). There were first freeze-dried, then ground and homogenized before analyses.

About 0.5 g of sediment was acidified using 1 mol L^{-1} HCl and heated overnight in a water bath at 50 °

C. The excess acid was washed away using ultrapure water (Williford et al., 2007). These samples were

155   weighed for TOC and $\delta^{13}C_{org}$ determinations. For TN and nitrogen stable isotopes ($\delta^{15}N$) analyses, we

used samples that were not acidified. TOC, TN, $\delta^{13}C_{org}$, and $\delta^{15}N$ measurements were carried out on an

elemental analyzer Elementar CHNOS coupled to an isotope ratio mass spectrometer (IRMS, Thermo,

Delta V advantage). The standard deviations for TOC, TN, $\delta^{13}C_{org}$, and $\delta^{15}N$ based on replicate analyses

were 0.02%, 0.005%, 0.2‰, and 0.2‰, respectively.

160   **3.4 Biomarker Analyses**

Biomarker analyses were completed at MED, SIO, MNR (Hangzhou, China). Before extraction,

internal standards 7-hexylnonadecane and cholest-5-en-3β-ol-D6 were added to about 5 g of freeze-dried

and homogenized sediment for quantification of HBIs and sterols, respectively. Extraction was

performed 3 times in an ultrasonic bath for 15 min using dichloromethane/methanol (2:1 v/v). The 3

165   extracts were combined and dried under a gentle nitrogen stream. Further separation was carried out by

adsorption chromatography on an open-column filled with SiO$_2$ using 2.5 ml n-hexane and 4 ml n-

hexane/ethyl acetate (70:30 v/v) to separate the hydrocarbons and sterols, respectively, from the total lipid extract. About 50 μl BSTFA (bis-trimethylsilyl-trifluoroacetamide) were added to the sterol fraction and heated at 70 °C for 1 hr for silylation.

170 Then, hydrocarbons and sterols were analyzed by gas chromatography (GC, Agilent Technologies 7890, 30 m HP-1MS column, 0.25 mm in diameter, and 0.25 μm film thickness) coupled to mass spectrometry (MS, Agilent 262 Technologies 5975C inert XL). A heating rate of 10 °C min^{-1} for the oven temperature was programmed from 40 °C to 300 °C and maintained at final temperature for 10 min. The ion source temperature was set at 250 °C and ionization energy at 70 eV for MS analyses (Belt et al.,

175 2007, Müller et al., 2009). Individual compounds were identified based on their retention time and mass spectra. Selective ion monitoring was used to detect the C_{25}-HBIs (*m/z* 350 for IP_{25}, *m/z* 348 for HBI-II, and *m/z* 346 for HBI-III) and the sterols (*m/z* 470 for brassicasterol (24-methylcholesta-5,22E-dien-3β-ol)), *m/z* 500 for dinosterol (4α,23,24R-trimethyl-5α-cholest-22E-en-3β-ol), *m/z* 396 for β-sitosterol (24-ethylcholest-5-en-3β-ol) and *m/z* 382 for campesterol (24-methylcholest-5-en-3β-ol). Concentrations of

180 HBIs were determined based on the area of individual compounds and that of the 7-hexylnonadecane (*m/z* 266) obtained by GC/MS. Similarly, sterol concentrations were calculated from the area of individual sterols and cholesterol-D6 (cholest-5-en-3β-ol-D6, *m/z* 464) (Belt et al., 2012, Müller et al., 2011). Concentrations of all biomarkers were normalized to TOC.

3.5 PIP_{25} Index and H-print

185 PIP_{25} indexes were calculated to estimate seasonal sea ice concentrations (Müller et al., 2011) using the following expression:

$$PIP_{25} = \frac{[IP_{25}]}{[IP_{25}] + [phytoplankton\ \ biomarker] * c} \tag{1}$$

$$where \quad c = \frac{mean\ \ IP_{25}\ \ concentration}{mean\ \ phytoplankton\ \ biomarker\ \ concentration} \tag{2}$$

Brassicasterol (B), dinosterol (D), and HBI-III (III) were used as a reference for pelagic phytoplankton

190 to calculate the P_BIP_{25}, P_DIP_{25}, and $P_{III}IP_{25}$ values, respectively.

The H-print values were also calculated to infer the relative contribution of pelagic and sympagic OC (Brown et al., 2014b, Koch et al., 2020).

$$H - print\% = \frac{[HBI - III]}{[IP_{25}] + [HBI - II] + [HBI - III]} \times 100 \tag{3}$$

Low H-print values are indicative of higher sympagic production while high H-print values point to prevalent pelagic algae.

3.6 Environmental dataset of surface sediment

Assessment of seasonal sea ice spatial distribution is based on the compilation of previously published surface sediment data from the ESS (HBIs, Su et al., 2022) and the CS (HBIs, Bai et al., 2019; $\delta^{13}C_{org}$, Wang et al., 2017) and new data from the CS and CP produced in this study. $\delta^{13}C_{org}$ data from the ESS are also new together with all data from the R1 core.

4. Results

4.1 Chronology of core R1
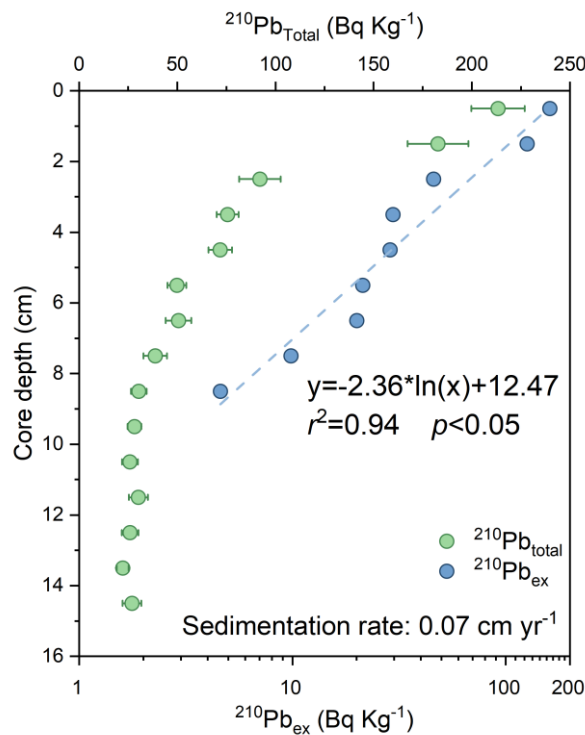
Figure 2. Downcore profile of $^{210}Pb_{total}$ (green circles) with the error range and $^{210}Pb_{ex}$ (blue circles) for ARC11-R1.

The activity of $^{210}Pb_{total}$ ranges from 22 to 214 Bq Kg^{-1}, with an average value of 64.30 Bq Kg^{-1} (Fig. 2). $^{210}Pb_{ex}$ decreases exponentially with increasing depth to reach negligible values around 9 cm. The calculated average sedimentation rate of R1 using the CF-CS model is estimated to 0.07 cm yr^{-1} (r^2=0.94, p<0.05), which gives a time span of about 200 years for the whole core. The ^{137}Cs profile (not shown)

Table 1. Summary of bulk parameters and biomarker data from surface sediment in the Chukchi Sea and Chukchi Plateau.

Station	Long.	Lat.	TOC (wt%)	TN (wt%)	$\delta^{13}C_{org}$ (‰)	$\delta^{15}N$ (‰)	IP$_{25}$ relative abundance[*]	HBI-II relative abundance[*]	HBI-III relative abundance[*]	Brassicasterol[*]	Dinosterol[*]	Campesterol+ β-sitosterol[*]
E1	-179.89	75.01	1.23	0.17	-23.72	9.42	1.58	1.23	0.17	25.34	3.11	189.29
P2-5	-163.68	76.60	0.87	0.12	-22.73	8.67	0.22	0.18	0.04	1.79	0.60	37.33
R5	-168.94	77.76	1.18	0.15	-23.54	9.05	0.52	n.d.	n.d.	3.05	0.92	44.19
E2	179.99	75.84	0.57	0.13	-22.99	8.92	3.90	n.d.	n.d.	20.07	3.59	127.45
R2	-168.92	75.61	0.96	0.18	-22.64	9.91	1.00	0.69	0.76	19.30	4.28	135.13
P3-7	-165.92	78.61	0.65	0.12	-22.26	8.01	n.d.	n.d.	n.d.	3.27	0.65	63.21
P1-6	-166.62	75.44	0.69	0.16	-23.13	9.44	1.00	0.59	1.47	7.85	2.81	86.21
Z4	-166.61	73.54	1.42	0.28	-22.89	8.74	5.49	6.52	3.06	21.89	7.04	141.89
Z3	-167.16	74.34	0.78	0.21	-22.52	9.41	4.45	4.32	2.31	97.67	24.09	528.94
P3-8	-162.58	78.36	0.61	0.12	-22.94	8.04	n.d.	n.d.	n.d.	5.56	1.02	79.41

n.d.: not detected

210 [*] in µg g^{-1} TOC

Table 2. Summary of bulk parameters and biomarker data from core ARC11-R1.

Core depth (cm)	Age (yr AD)	TOC (wt%)	TN (wt%)	C/N Ratio	$\delta^{13}Corg$ (‰)	$\delta^{15}N$ (‰)	IP$_{25}$ Relative abundanc[*]	HBI-II Relative abundance[*]	HBI-III Relative abundance[*]	Brassicasterol[*]	Dinosterol[*]	Campesterol+ β-sitosterol[*]
0-1	2013	1.18	0.18	7.76	-23.51	9.35	0.45	0.77	0.51	40.04	8.73	86.00
1-2	2000	1.13	0.17	7.66	-23.79	9.32	0.66	0.88	0.62	34.25	5.63	69.22
2-3	1986	0.94	0.15	7.15	-23.46	9.05	0.82	0.93	0.47	33.61	5.09	78.85
3-4	1972	0.95	0.13	8.39	-24.40	8.48	0.38	0.53	0.23	21.25	3.16	52.94
4-5	1959	0.73	0.12	7.27	-24.17	7.66	0.22	0.44	0.16	16.78	3.53	36.75
5-6	1945	0.77	0.11	7.94	-24.25	7.53	0.24	0.43	0.16	14.58	3.03	28.39
6-7	1932	0.81	0.11	8.62	-24.27	7.17	0.85	0.71	0.23	14.88	3.00	35.05
7-8	1918	0.77	0.11	8.41	-24.30	6.56	0.39	0.74	0.31	15.18	2.75	33.48
8-9	1904	0.85	0.10	9.49	-24.63	6.22	0.23	0.75	0.40	16.02	2.76	23.36
9-10	1891	0.81	0.11	8.60	-24.63	6.64	0.24	0.98	0.26	14.64	3.31	20.77
10-11	1877	0.84	0.11	8.75	-24.87	6.67	0.21	0.93	0.27	13.14	3.19	30.66
11-12	1864	0.86	0.11	8.96	-24.76	6.74	0.18	1.01	0.38	13.03	2.69	23.97
12-13	1850	0.79	0.11	8.59	-24.93	6.38	0.19	0.94	0.42	12.37	2.78	16.89
13-14	1837	0.73	0.09	9.12	-25.19	6.31	0.19	0.63	0.20	8.77	2.46	12.02
14-15	1823	0.71	0.09	9.16	-25.07	5.43	0.77	0.21	0.30	6.51	2.40	14.62

[*] in µg g^{-1} TOC

further supports the ^{210}Pb dating. This value falls within the range reported by Cooper and Grebmeier (2018) in a Chukchi Shelf core (0.03-0.37 cm yr^{-1}) and is slightly lower than found at the ARC4-C07 core (0.09 cm yr^{-1}, Bai et al., 2022) and ARA01B-03MUC core (0.09 cm yr^{-1}, Kim et al., 2019) both located to the south (Fig. 1).

215
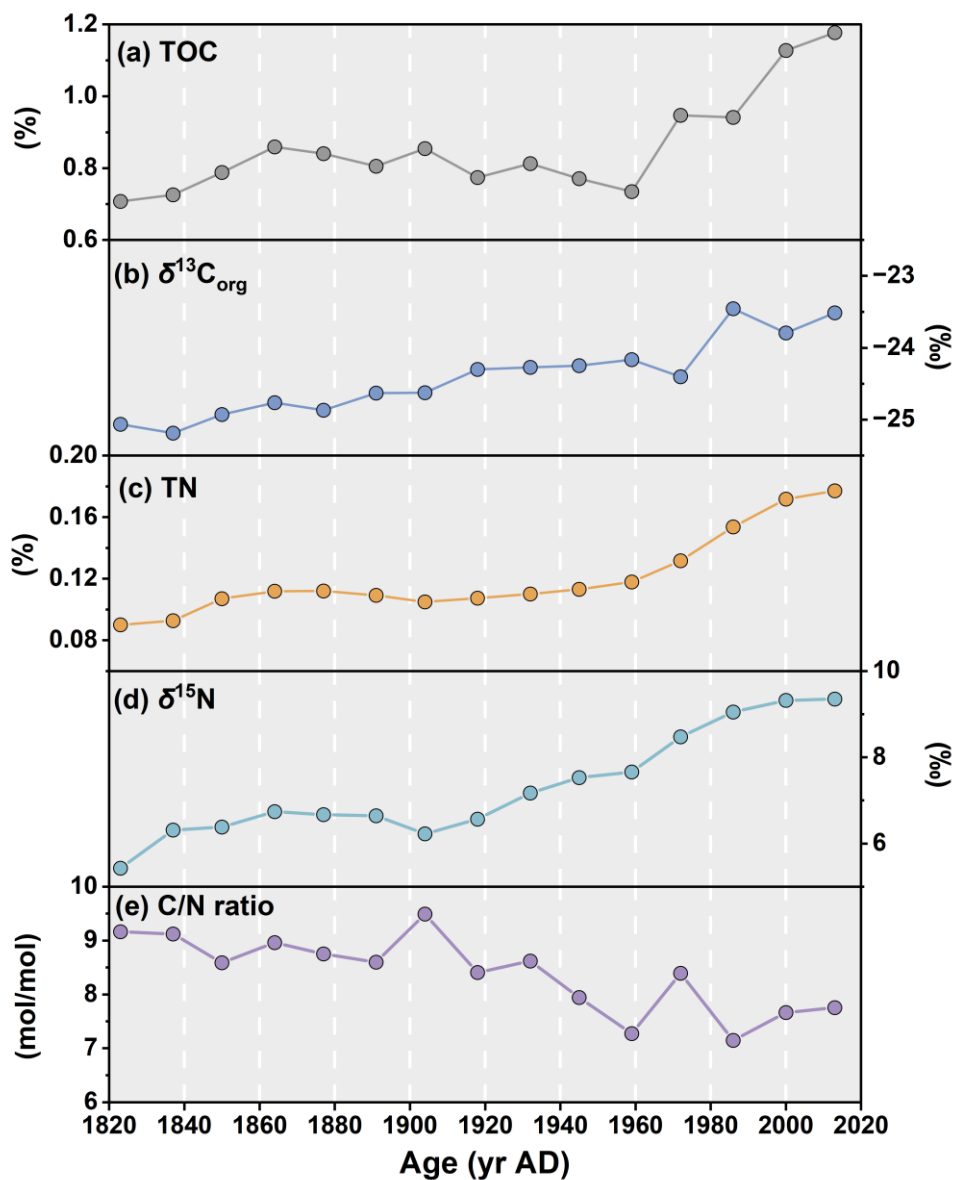
Figure 3. Downcore profiles of (a) Total Organic Carbon, TOC in %, (b) Organic carbon isotopic composition ($\delta^{13}C_{org}$) of the TOC in ‰, (c) Total Nitrogen, TN in %, (d) nitrogen isotopic composition ($\delta^{15}N$) in ‰, and (e) C/N ratio in the ARC11-R1 core.

220 **4.2 Proxy data**

4.2.1 Surface sediments

The TOC and TN of surface sediments range from 0.57% to 1.42% and from 0.12% to 0.28% respectively (Table 1, Fig. S1). $\delta^{13}C_{org}$ varies from -23.7‰ to -22.0‰ and $\delta^{15}N$ from 8.01‰ to 9.91‰. Both HBIs and pelagic phytosterol concentrations showed a gradual decrease from the shelf to the northern CP. The concentrations of HBI-II and HBI-III reached their detection limit at around 76 °N, whereas for IP$_{25}$ this limit is achieved north of 78 °N. By contrast, brassicasterol and dinosterol were detected in all samples with highest values recorded at the shelf edge. Terrestrial sterols (β-sitosterol and campesterol) showed high values over the shelf and minimum ones at the northern end of the CP.
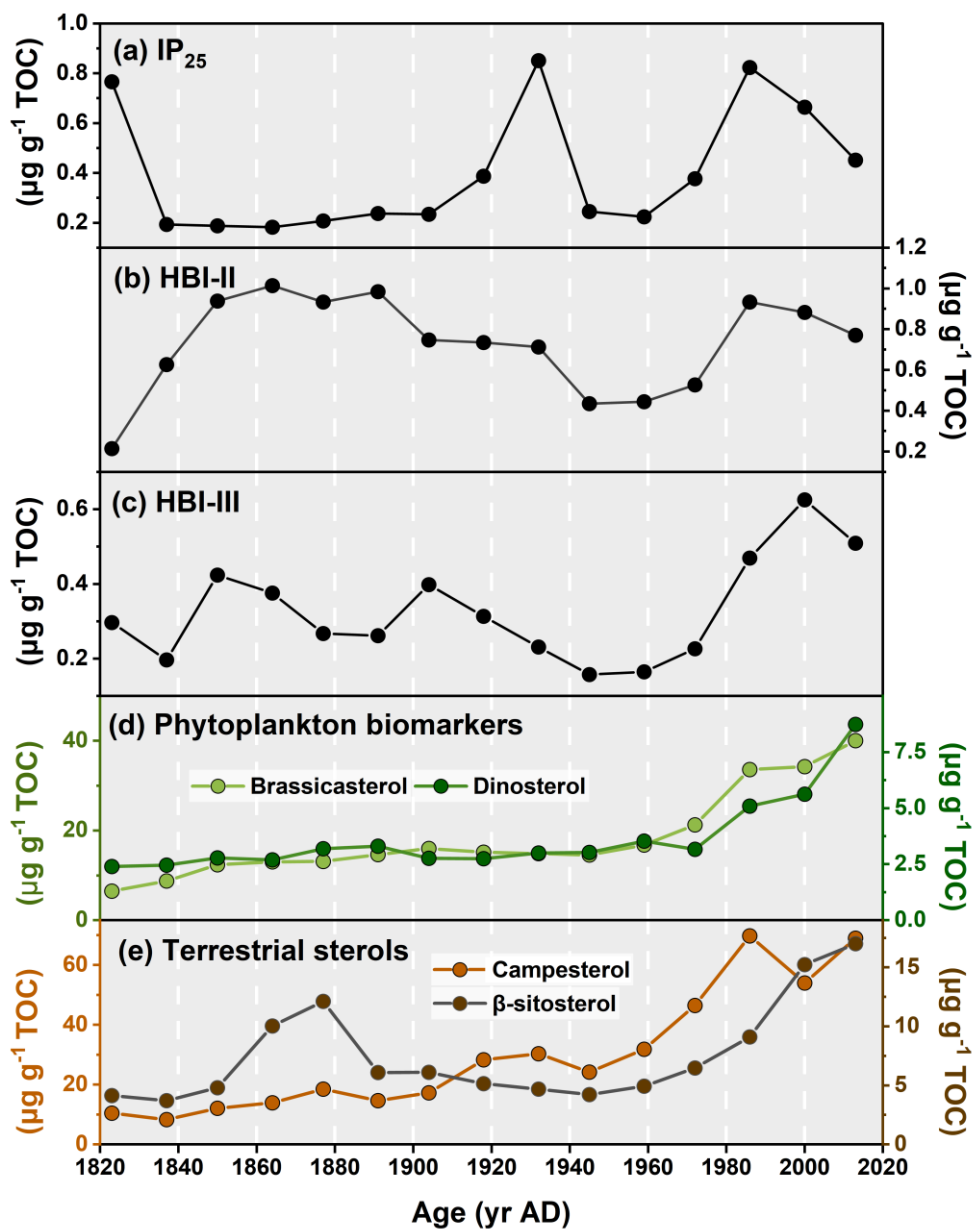
Figure 4. Downcore profiles of (a) IP$_{25}$, (b) HBI-II, (c) HBI-III, (d) brassicasterol and dinosterol, and (e) campesterol and β-sitosterol in core ARC11-R1.

4.2.2 ARC11-R1 core

The TOC and TN downcore profiles over the last 200 years both show increasing trends towards present (r^2=0.88, p<0.01) with values varying from 0.71% to 1.18% and from 0.09% to 0.18%, respectively (Table 2, Fig. 3a and c). TOC exhibits a minimum end of the 1950s and rapidly increases thereafter. Downcore values of C/N ratios show a gradual decrease from 9.2 to 7.6 while $\delta^{13}C_{org}$ consistently increases from -25.07‰ to -23.46‰ in the 1980s (Table 2, Fig. 3b and d). $\delta^{15}N$ exhibits constant values until the early 1900s after which it gradually increases and reaches a maximum at the top of the core (9.35‰; Table 2, Fig. 3d).

The IP_{25} concentrations span from 0.18 to 0.85 µg g^{-1} TOC with highest values found in the 1930s and after the1980s (Fig. 4a). Brassicasterol and dinosterol both exhibit increasing abundances over time (Fig. 4d, r^2=0.85, p<0.01), with brassicasterol being notably more abundant (6.51 µg g^{-1} TOC to 40.04 µg g^{-1} TOC) than dinosterol (2.40 µg g^{-1} TOC to 8.73 µg g^{-1} TOC; Fig. 4d). Finally, terrestrial sterols slowly increase from 1820s to present in R1 core (campesterol: 10.47 µg g^{-1} TOC to 68.98 µg g^{-1} TOC, β-sitosterol: 4.15 µg g^{-1} TOC to 17.02 µg g^{-1} TOC; Fig. 4e).

5 Discussion

5.1 Reconstruction of sea ice conditions

Sympagic biomarker IP_{25} concentrations (0.40 $\pm$ 0.25 µg g^{-1} TOC, mean $\pm$ S.D.) were lower throughout the R1 core than found over the same period in the ARA01B-03MUC (0.96 $\pm$ 0.72 µg g^{-1} TOC, Kim et al., 2019) and ARC04-C07 cores (1.29 $\pm$ 1.19 µg g^{-1} TOC, Bai et al., 2022), both located south of R1 core (Fig. S2). Decreasing sympagic biomarker concentrations with increasing latitude likely reflect lower export of sympagic OC to the sea floor due to higher sea ice cover in the North. However, this interpretation does not rule out a possible contribution of analytical methods and/or regional depositional conditions (Belt, 2018). The box-plot in Fig. S2 also points to higher variability at the two further south sites possibly reflecting sea ice edge variations. The presence of IP_{25} throughout R1 indicates seasonal sea ice cover and/or sea ice edge conditions since the 1820s at this location. While Bai et al. (2022) reported parallel trends of IP_{25} and HBI-II throughout core ARC4-C07, this feature is only observed after the 1930s in core R1 (Fig. 4a and b). Indeed, before 1930s, these two HBIs show opposite behavior. The reasons for this discrepancy are not entirely clear and few data exist to explore in depth

possible explanations. It is worthy to note that both HBIs in the sediment trap at the DM station (74 °N) shown similar production/export behavior (Bai et al., 2019). HBI-II is commonly found in Southern Ocean sediments, unlike IP_{25}, where its production has been attributed to the sea ice diatom *Berkeleya adeliensis* (Belt et al., 2016; Brown et al., 2014a). It was also noted that *B. adeliensis* tends to preferentially flourish in platelet ice, particularly in coastal settings, leading to link its occurrence to landfast sea ice associated with freshwater discharge in Southern Ocean sediments (Belt, 2018, 2019). The divergent behavior the HBI-II and IP_{25} prior the 1930s could thus indicate variable sea ice conditions with a possible contribution of drifting ice from coastal areas of the ESS.

Combined IP_{25} and pelagic phytoplankton biomarkers were investigated to quantify downcore seasonal sea ice cover. To test the sensitivity of PIP_{25} to *c*-factor, PIP_{25} values were calculated using different *c*-factors of Xiao et al. (2015a) and Smik et al. (2016), and *c*-factor calculated from surface sediments collected from the CS and R1 for this study. The estimated PIP_{25} values were found to be consistent with each other with comparable fluctuations (Fig. S3). Additionally, a previous study in the same region suggested that the PIP_{25} derived sea ice reconstructions were more reliable by using *c*-factors from the Pan-Arctic database (Kim et al., 2019). Thus, in this study, P_BIP_{25}, $P_DIP_{25,}$ and $P_{III}IP_{25}$ were calculated using surface sediment balance factors *c* of 0.02, 0.11 (Xiao et al., 2015a) and 0.63 (Smik et al., 2016), respectively. All indexes show similar trends (Fig. S3) reflecting the strong correlation between brassicasterol, dinosterol and HBI-III (Fig. 5 and S4; all: $r > 0.63$, $p < 0.01$). Only in the 1820s and 1930s are PIP_{25} values above the threshold of 0.75 indicative of permanent sea ice according to Müller et al. (2011) (Fig. 5).

Between the 1820s and 1850s, all PIP_{25} values steeply drop suggesting rapid sea ice retreat. Then, P_BIP_{25} and P_DIP_{25} show rather stable values till the beginning of the 20th century whereas $P_{III}IP_{25}$ slowly increase (Fig. 5). All three PIP_{25} indexes point to seasonal sea ice or marginal ice zone conditions. Higher amounts of HBI-III and $P_{III}IP_{25}$ values may indicate sea ice edge conditions. Sediment trap data from the Northwind Ridge and slope of the East Siberian Sea show high levels of brassicasterol till late summer/early autumn when ice free conditions are reached, whereas HBI-III is close to the detection limit in mid-summer when sea ice has melted (Bai et al., 2019, Gal et al., 2022). This result further confirms that HBI-III producers proliferate at the sea ice edge rather than in ice free waters. From 1850s

to 1910s, both P_BIP_{25} and P_DIP_{25} were below 0.5, pointing to less and variable sea ice cover than the end of early 19th century, contrary to observations indicating high sea ice cover (Walsh et al., 2017). $P_{III}IP_{25}$ falls in a higher sea ice cover range. Increasing P_DIP_{25} and P_BIP_{25} values between 1910s and 1930s occur while observations indicate a significant reduction of sea ice from permanent to marginal sea ice (Walsh et al., 2017). Bias to higher sea ice cover estimates using $P_{III}IP_{25}$ is explained by HBI-III production taking place at the ice edge rather than ice-free conditions. Low concentrations of IP_{25} and phytoplankton biomarkers during this period may also uncertainties in the calculation of the PIP_{25} index (Fig. 6) as suggested by previous studies (Müller et al., 2011; Xiao et al., 2015b). Observation data of September sea ice extent since 1850 in the Chukchi Sea (Walsh et al., 2017) also supports high sea ice conditions between 1820s and 1930s (Fig. 5).
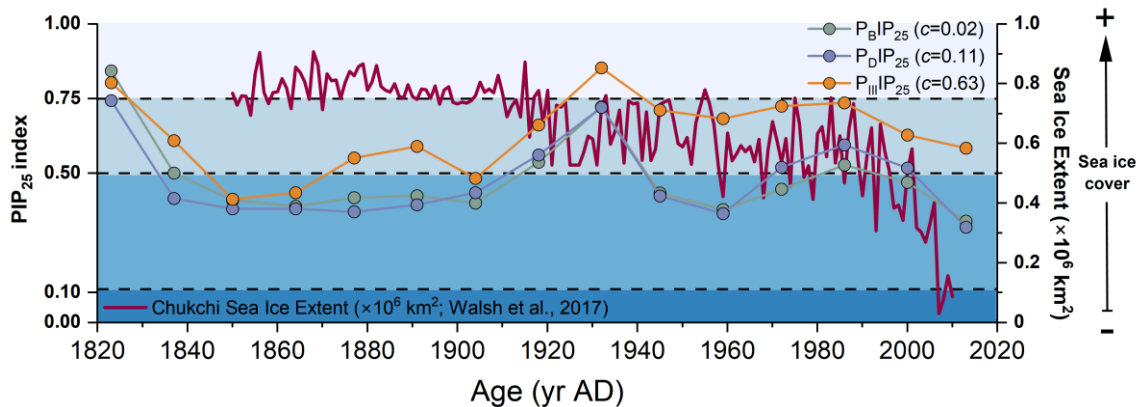
Figure 5. PIP_{25} index using brassicasterol (in green, P_BIP_{25}, c = 0.02 as calculated by Xiao et al. (2015a)), dinosterol (in purple, P_DIP_{25}, c = 0.11 as calculated by Xiao et al. (2015a)), and HBI-III (in orange, $P_{III}IP_{25}$, c = 0.63 as calculated by Smik et al (2016)) and September sea ice extent record for the Chukchi Sea (red line, Walsh et al., 2017).
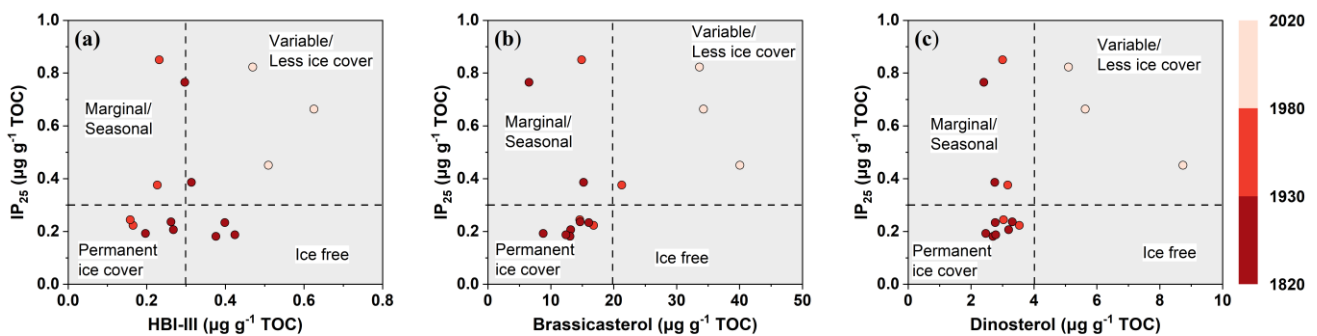
Figure 6. Cross-plot between concentrations of IP_{25} and phytoplankton biomarkers ((a) HBI-III, (b) brassicasterol and (c) dinosterol, respectively) in the ARC11-R1 core distinguishing between different spring/summer sea ice condition zones. The gradient from dark to light red represents periods of 1820-1930, 1930-1980, and 1980-2020, respectively.

After 1930s, $P_{III}IP_{25}$ gradually decrease to ca 0.7 while P_BIP_{25} and P_DIP_{25} drop to lower values around 0.4 till the 1960s to then slightly increased until the 80s -90s when P_BIP_{25} and P_DIP_{25} exceed the seasonal sea ice threshold value (0.5) and $P_{III}IP_{25}$ that of nearly permanent sea ice at approximately 0.75. In this time interval (1930s - 1980s), low IP_{25} and increasing brassicasterol in cores ARC4-C07 and ARA01B-03MUC suggest enhanced sea ice melting and the northward retreat of the summer ice edge (Fig. S5). From 1980s to present, P_BIP_{25} and P_DIP_{25} continued to decrease but at a faster rate (Fig. 5 and 7a, b, c) emphasizing the unprecedented decline of seasonal sea ice over the last 30 years, as also found by Astakhov et al. (2019) and shown by remote sensing data (Walsh et al., 2017, Wang et al., 2019b).
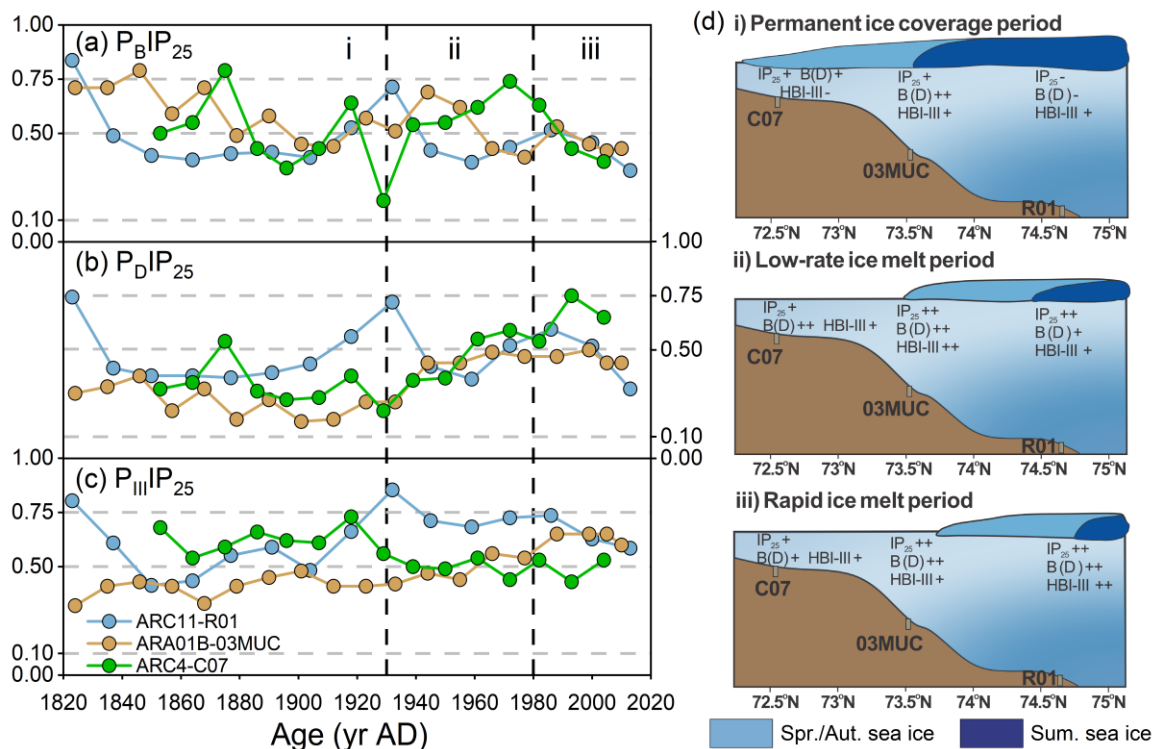
Figure 7. Downcore profiles of (a) PIP$_{25}$ index using brassicasterol (P$_B$IP$_{25}$), (b) dinosterol (P$_D$IP$_{25}$) and (c) HBI-III (P$_{III}$IP$_{25}$) in the core ARC04-C07 (green, Bai et al. 2022), ARA01B-03MUC (yellow, Kim et al. 2019) and ARC11-R1 (blue). i, ii and iii in (a), (b) and (c) represent different sea ice cover scenarios, which are schematically illustrated in (d). The color of sea ice in (d) represents the different sea ice cover: light blue for spring/autumn sea ice, and dark blue for summer sea ice.

In summary, the downcore profiles of seasonal sea ice proxies over the last 200 years evidence (Fig. 7d): i) reconstructed lower sea ice cover contrasting with nearly permanent sea ice observation record between the 1820s and 1930s, implying the limitation of PIP$_{25}$ index under nearly permanent sea ice; ii) from 1930s to 1980s, the seasonal sea ice slowly retreated to the north and the summer sea ice edge gradually reached the location of the R1 core; iii) a strong reduction sea ice cover with summer sea ice

edge conditions being reached since the 1980s at our core site. Finally, our findings highlight the need to further investigate the potential value of HBI-II in the Arctic Ocean to track drifting and landfast ice from coastal regions under freshwater discharge influence.

5.2 Organic carbon variability in response to sea ice change

5.2.1 Modern sources of organic carbon

The loss of sea ice is the most remarkable manifestation of global warming in the Arctic that has profound impacts on the carbon cycle. The most obvious one is the shift of the primary production pattern as a result of light and nutrient supply changes. Enhanced riverine inputs of terrestrial organic matter also affect the nature and amount of organic carbon reaching the Arctic Ocean. In this section, we investigate OC compositional changes over the past 200 years in relation with sea ice conditions by distinguishing three major carbon pools, e.g., sympagic, pelagic and terrestrial. We use the H-print ratio as a complementary indicator to PIP_{25} to discriminate pelagic and sympagic marine sources (Brown et al., 2014b; Brown and Belt, 2017; Koch et al., 2020). As shown in figure 8a, high values of H-print (>80%) occur in the western CS where marine phytosterols are high (dinosterol concentrations >5 µg g^{-1} TOC and brassicasterol concentrations >100 µg g^{-1} TOC, Su et al., 2022). Intermediate values (30%-60%) are roughly lying between the 1979 and 2019 isolines of the September minimum ice edge, denoting mixed pelagic and sympagic productions (Fig 8a). Minimum H-print values are found in coastal sediments along the western ESS and suggest freshwater discharge, by lowering water salinity, can suppress HBI-III production (Su et al., 2022) (Fig. 8a). At higher latitudes, low H-print values are likely reflecting light limitation due to nearly permanent sea ice cover (Fig. 8a).

Earlier studies in Arctic Eurasia estuary sediments have reported $\delta^{13}C_{org}$ values ranging from -27.8‰ to -24.7‰ (Bröder et al., 2019; Tesi et al., 2014). Lowest values (-27.5‰ to -26‰, Fig. 8b) are found in the western ESS shelf sediments receiving land-derived material from the Indigirka and Lena rivers in agreement with previous data (-27.5‰ to -25.5‰, Bröder et al., 2019). Apart from permafrost thawing, sea ice retreat likely accelerated coastal erosion contributing to the transfer of allochthonous material towards the Arctic Ocean (Overeem et al., 2011). The $\delta^{13}C_{org}$ values of organic matter produced by phytoplankton in the Arctic Ocean vary around -24 ± 3‰ (Stein et al., 2004; Vonk et al., 2012), which are similar to those found in saline waters of the western CS characterized by high pelagic production

350 (Fig. 8b). Enriched $\delta^{13}C_{org}$ values (-22‰ to -20.5‰) are also observed in the marginal ice zone/seasonal

sea ice zone of the CS (Fig. 8b) where sea ice plankton production is significant, which is in accordance

with values reported in sea ice (-23.6‰ to -18.3‰) (Schubert and Calvert, 2001).

$\delta^{13}C_{org}$ and H-print were combined to discriminate among autochthonous and allochthonous sources

of OC in our surface sediments. As illustrated by the scatter plot in figure 8c, a three- end-member

355 distribution emerged from the relationship between these 2 parameters and summer sea ice concentration

(SuSIC) demonstrating their potential to differentiate sympagic, pelagic and terrestrial OC in our dataset.

The site symbolizing the sympagic end-member is located at the sea ice edge where sea ice phytoplankton

production is high. Coincidentally, its $\delta^{13}C_{org}$ value (-20.5‰) falls within the range of values reported in

the lowermost 10 cm of sea ice cores (-23.6‰ to -18.3‰, Schubert and Calvert, 2001) and close to the

360 mean $\delta^{13}C_{org}$ value of sedimentary IP_{25} (-19.3‰±2.3‰, Belt et al., 2008). The terrigenous end-member

is consistently represented by sites located in estuarine zones or where land-derived supply dominates.

Pelagic end-member values (-23.5‰) are encountered in the western CS where phytoplankton

productivity is the highest and the influence of terrigenous and sea ice carbon less pronounced. This more

depleted value as compared to IP_{25} is consistent with the latter being produced in sea ice. Indeed, the

365 $\delta^{13}C_{org}$ of the two marine components also depends on pCO_2. Higher pCO_2 in surface waters may result

in lower $\delta^{13}C_{org}$ in pelagic marine algae OC while sea ice diatoms are relatively enriched in $\delta^{13}C_{org}$ due

to potentially limited CO_2 in sea ice (Tortell et al., 2013). It should be pointed out that our surface

sediment dataset covers the nearshore, shelf and basin regions, with different deposition rates therefore

the OC source apportionment reflect several tens to hundred years, depending on the location (Bröder et

370 al., 2016; Baskaran and Naidu, 1995; Vonk et al., 2012; Li et al., 2020). Nevertheless, H-print, $\delta^{13}C_{org}$

and SuSIC successfully discriminate OC sources.

Based on these results, a ternary mixing model was used to calculate the relative contribution of

sympagic, pelagic, and terrestrial sources in our surface sediments (Fig. 8c and Fig. S6; Table S1) using

the following equation:

$$\delta^{13}C_{sample} = f_{sym} \times \delta^{13}C_{sym} + f_{pela} \times \delta^{13}C_{pela} + f_{terr} \times \delta^{13}C_{terr} \tag{4}$$

$$H - print_{sample} = f_{sym} \times H - print_{sym} + f_{pela} \times H - print_{pela} \tag{5}$$

$$f_{sym} + f_{pela} + f_{terr} = 100\% \tag{6}$$

375   where f_{sym}, f_{pela}, and f_{terr} are the sympagic, pelagic, and terrestrial fractions of OC, respectively. The $\delta^{13}C_{org}$

end-members for used for the sympagic end-member at 0% for H-print is -20.5‰. The pelagic $\delta^{13}C_{org}$

end-member at 100% for H-print is -23.5‰. The terrestrial $\delta^{13}C_{org}$ end-member is -27.5‰.

5.2.2 Source and burial of organic carbon change over the last two centuries

     In this section, we examine the temporal evolution of sympagic, pelagic and terrestrial fractions of

380   OC calculated with our ternary mixing model and end-member values, with changing sea ice conditions

over the last two centuries. Figure 9a shows that TOC values slowly increase between 1820 and 1860

and remain relatively stable around 0.8% until 1960 where they increase rapidly to reach their highest

levels (1.17%) at the core-top, falling in the range reported in the surface sediments of the CS shelf and

CP (1.25% to 2.56%, Goñi et al., 2013; 0.31% to 1.73%, Ji et al., 2019). This trend is paralleled by

385   increasing $\delta^{13}C_{org}$ values (Fig. 9a), suggesting that higher TOC may be related to enhanced marine

production (primary and secondary). Indeed, sea ice retreat and increase ice free conditions are expected

to result in higher rates of primary production due to higher light penetration and more nutrients supply

both from river and via wind driven mixing. In addition, a longer season of production will also

subsequently enhanced production and export to the sea floor (Ouyang et al., 2022; Zhuang et al., 2022).
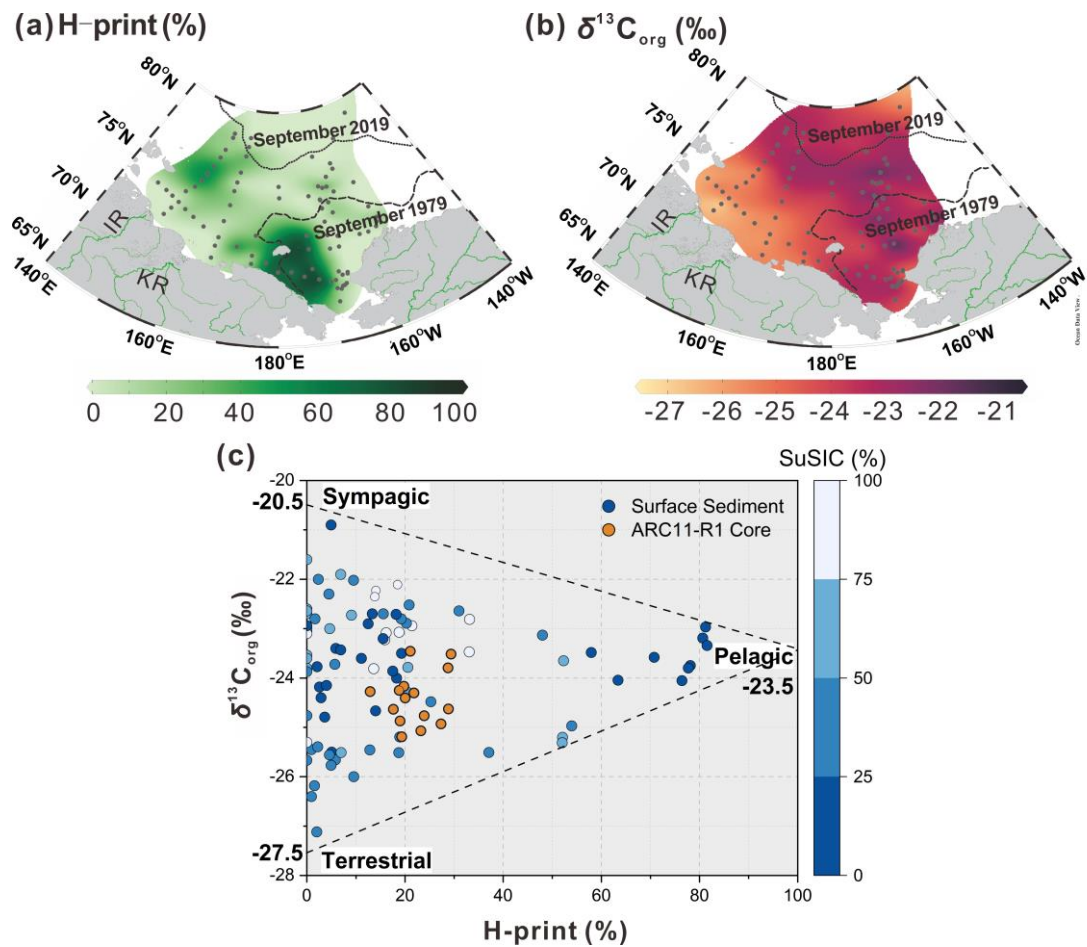
Figure 8. Distribution of (a) H-print and (b) $\delta^{13}C_{org}$ in the surface sediments of the ESS and CS. (c) Cross-plot of values of $\delta^{13}C_{org}$ and H-print for surface sediments. The gradient from dark blue to white represents SuSIC (Summer Sea Ice Concentration, NSIDC) from 0-20%, 20-40%, 40-60%, 60-80% and 80-100%, respectively, and ARC11-R1 core (in orange). The $\delta^{13}C_{org}$ end-members for the sympagic end-member at 0% for H-print is -20.5‰. The pelagic $\delta^{13}C_{org}$ end-member at 100% for H-print is -23.5‰. The terrestrial $\delta^{13}C_{org}$ end-member is -27.5‰. The dotted and dashed lines in black represent the 20% isolines of September sea ice concentration for the 2019 and 1979, respectively.

Table 3. Overall organic carbon composition of core ARC11-R1 (relative portion, f_{oc} (%), and absolute content, OC (mg g^{-1} d. w.)).

Core depth (cm)	Age (yr AD)	f_{sym} (%)	f_{pela} (%)	f_{terr} (%)	OC$_{sym}$ (mg g^{-1} d. w.)	OC$_{pela}$ (mg g^{-1} d. w.)	OC$_{terr}$ (mg g^{-1} d. w.)
0-1	2013	40.14	29.40	30.45	4.73	3.46	3.59
1-2	2000	36.50	28.77	34.72	4.12	3.24	3.92
2-3	1986	45.70	21.09	33.20	4.30	1.99	3.13
3-4	1972	32.77	20.05	47.18	3.10	1.90	4.47
4-5	1959	36.32	19.79	43.89	2.67	1.45	3.22
5-6	1945	35.68	18.83	45.49	2.75	1.45	3.50
6-7	1932	38.71	12.9	48.39	3.15	1.05	3.93
7-8	1918	33.23	21.83	44.94	2.57	1.69	3.48
8-9	1904	24.57	28.86	46.57	2.10	2.46	3.98
9-10	1891	30.89	17.64	51.47	2.47	1.42	4.14
10-11	1877	26.71	19.00	54.29	2.24	1.60	4.56
11-12	1864	25.42	23.91	50.67	2.18	2.05	4.35
12-13	1850	21.11	27.34	51.55	1.66	2.15	4.06
13-14	1837	21.96	19.34	58.70	1.59	1.40	4.26
14-15	1823	21.48	23.23	55.29	1.51	1.64	3.91

The C/N ratios are higher than the Redfield ratio over the entire core and show a decreasing trend (Fig. 9b), in agreement with diminishing contribution of terrestrial with respect to marine OC sources. The mean f_{terr} is relatively high throughout the R1 core (46.45% ± 8.20%, Fig. 9c and Table 3) but decrease from 58.70% to 30.45%. Although R1 is located rather far from the continent, these estimates suggest efficient transport pathways of land-derived organic matter towards the open sea such as drifting sea ice (Jia et al., 2020) or wave action remobilizing and transporting shelf sediments to the ocean interior (Vonk et al., 2012). Time series sediment traps evidenced high and long-standing terrigenous material advection by lateral transport controlled by Chukchi Slope Current and mesoscale eddies in winter in this region (Onodera et al., 2021; Watanabe et al., 2014; Watanabe et al., 2022). Figure 9c also shows that since the 1960s, there has been a significant decline in the share of terrigenous OC with the enhanced loss of sea ice of the last 60 years, and subsequent rise of productivity of marine and sea ice diatoms. By contrast, ARC4-C07, the core located to the southeast of R1 (Fig. 1), exhibits a trend of enhanced land-sourced input in recent years (Bai et al., 2022). The different trend of the terrigenous OC components of these two cores might be related to the weakening of sediment-laden sea ice transport to higher northern latitudes due to its earlier melting.
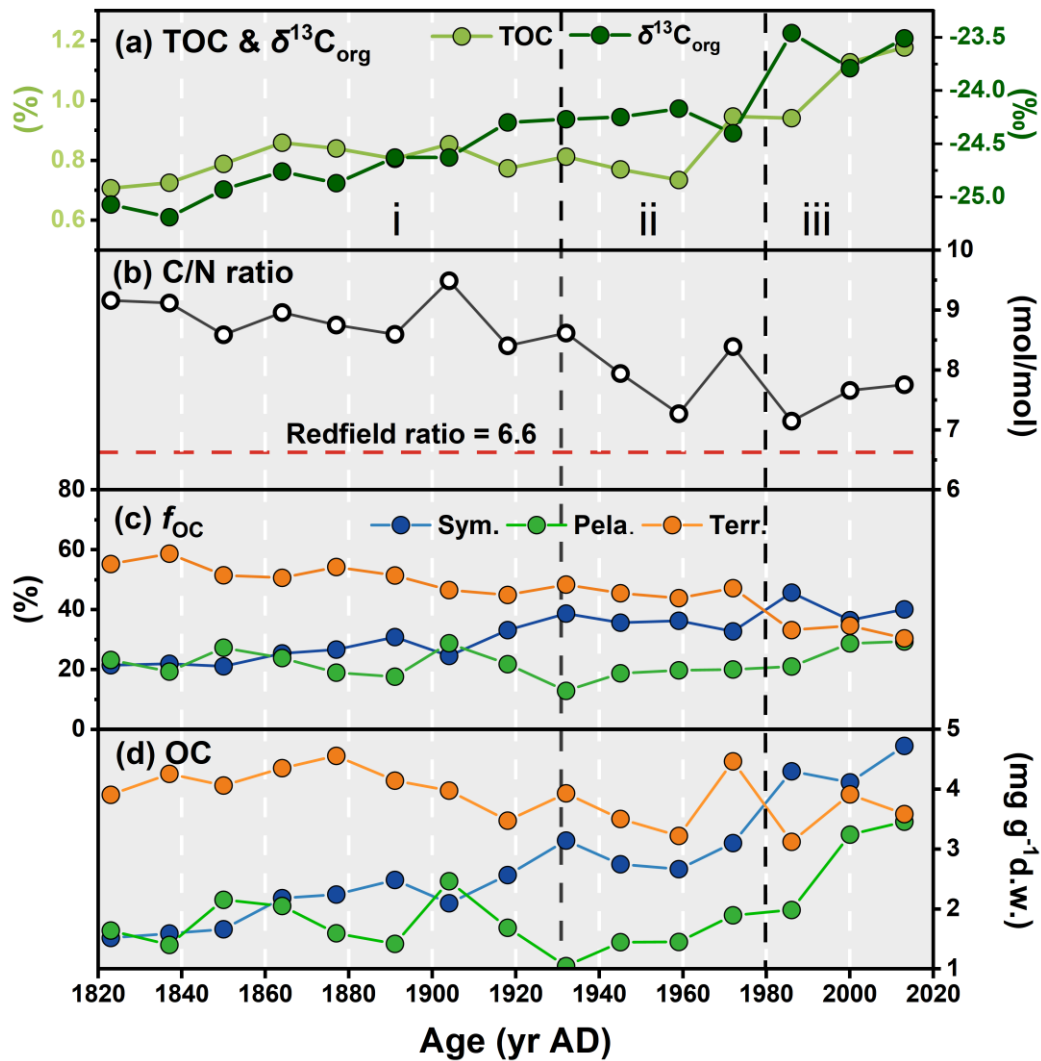
Figure 9. Downcore profiles of (a) TOC and $\delta^{13}C_{org}$, (b) C/N ratio, and (c) Proportion of the overall OC from each source (f_{OC}, calculated based on $\delta^{13}C_{org}$ and H-print), and (d) OC (mg g^{-1} d. w., dry weight) in the ARC11-R1 core. In (c) and (d), blue, green, and orange dots represent the sympagic, pelagic and terrestrial carbon input, respectively.

From the 1820s to 1930s, pelagic and sympagic OC are found in comparable amounts in the sediments (2.17 ±0.53 mg g^{-1} d. w. sediment and 1.72 ±0.46 mg g^{-1} d. w. sediment, respectively; Fig. 9d and Table 3), but from the 1930s to 1980s, the content of sympagic OC increase by nearly 50% to 3.10 mg g^{-1} d. w. sediment (Fig. 9d). However, pelagic phytoplankton growth also shows rising values but remain lower than sympagic OC possibly because of surface freshening limiting nutrient supply (Arrigo et al., 2008). After the 1980s, when the minimum ice edge reached R1 and the ice-free period prolonged in the northern CS (Astakhov et al., 2019), the sympagic and pelagic productions depict a final increase and superseding terrestrial OC (Fig. 9c and 9d). The high $\delta^{15}N$ data during this period suggest enhanced stratification most likely due to surface freshening (Fig. 3d) which gradually shifted the limiting factor of marine pelagic production from light to nutrients availability (Ardyna and Arrigo, 2020;

Lannuzel et al., 2020).

6 Conclusions

H-print and $\delta^{13}C_{org}$ values from 83 surface sediments were used to diagnose OC sources across the western Arctic Ocean and how they are influenced by sea ice extent. $\delta^{13}C_{org}$ values were consistently

440 generally lower in the southern coastal and shelf sediments where riverine terrigenous inputs are stronger, while heavier $\delta^{13}C_{org}$ were found at offshore sites of the northern CS and ESS where pelagic and/or sympagic productions are significant. Combining $\delta^{13}C_{org}$ and H-print enabled to draw an inventory of terrestrial, sympagic and marine pelagic OC in northern CS sediments using a ternary mixing model which was then applied to the ARC11-R1 core to reconstruct the temporal evolution of the OC content

445 since 1820 as the sea ice retreat.

Our results demonstrate that over the last 200 years the northern CS experienced nearly permanent sea ice conditions between 1820s and 1930s followed by a period of gradual melting to reach marginal sea ice conditions (1930s-1980s). The most recent decades were marked by the accelerated decline of sea ice (1980s - present) leading to shifts in primary production that, in turn, impacted the composition

450 and burial of OC in Arctic sediments from coastal to open sea areas. Our data show that with the loss of sea ice, the fraction of terrigenous OC decreased while marine pelagic and sympagic OC export and sequestration in the deep-ocean increased. Since the beginning of the 21st century the three OC pools at the core site are comparable in size while 200 years ago OC was predominantly of terrestrial origin. In the future, with rising temperature and reduced sea ice, primary production in the northern CS may

455 however become nutrients limited as a result of freshening and ocean stratification, and phytoplankton populations will likely undergo further alteration with subsequent changes in CO_2 drawdown.

Data availability.

All data that support the findings of this study are included within the article and supplement.

460 **Author contributions.**

L.S., J.R. and J.C. designed the study and wrote the manuscript with contribution of M.-A.S., Y.B., Z.L., R. Z., H.J., A.A.S. and X.S. L.S. and R. Z. contributed the biomarker analyses and the determination of bulk parameter. J.R. retrieved the environmental data from different database while X.H. carried out the age model estimate of R1. All authors contributed to the final version of the manuscript.

465

Competing interests. The authors declare that they have no conflict of interest.

Acknowledgements.

We are grateful to the captain, crewmembers and scientific party of the R/V *Xuelong 2* and R/V *Akademik*

470 *M.A. Lavrentiev* for their professional sampling work. We are indebted to Zhi Yang and Qianna Chen of Second Institute of Oceanography for their kind help in the bulk data measurement. Vincent Klein of Sorbonne University is also thanked for technical assistance. We are also grateful to Sabine Schmidt of University of Bordeaux for her suggestions on the age model. Two anonymous reviewers are acknowledged for their constructive suggestions.

475

Financial support. This study is financially supported by the National Natural Science Foundation of China (Nos. 41941013, 42076241, 41976229, 41606052, 42076242), the National Key Research and Development Program of China (Nos. 2019YFE0120900, 2019YFC1509101) and the Marine S&T Fund of Shandong Province for Pilot National Laboratory for Marine Science and Technology (Qingdao; No.

480 2018SDKJ0104-3). The expedition work was partly supported by the Ministry of Sciences and Education of the Russian Federation (Project 121021700342-9).

References

Ardyna, M. and Arrigo, K.R.: Phytoplankton dynamics in a changing Arctic Ocean, Nat. Clim. Change, 10(10), 892-903, https://doi.org/10.1038/s41558-020-0905-y, 2020.

485   Arrigo, K.R., van Dijken, G. and Pabi, S.: Impact of a shrinking Arctic ice cover on marine primary production. Geophys. Res. Lett., 35(19), https://doi.org/ 10.1029/2008gl035028, 2008.

Arrigo, K.R. and van Dijken, G.L.: Continued increases in Arctic Ocean primary production, Prog. Oceanogr., 136, 60-70, https://doi.org/ 10.1016/j.pocean.2015.05.002, 2015.

Astakhov A.S., Bosin A.A., Liu Y.G., Darin A.V., I.A. Kalugin, Artemova A.V., Babich V.V., Melgunov 490   M.S., Vasilenko Yu.P., VologinaE.G.: Reconstruction of ice conditions in the northern Chukchi Sea during recent centuries: Geochemical proxy compared with observed data. Quat. Int., 522, 23-37, https://doi.org/10.1016/j.quaint.2019.05.009, 2019.

Bai, Y., Sicre, M.-A., Chen, J., Klein, V., Jin, H., Ren, J., Li, H., Xue, B., Ji, Z., Zhuang, Y. and Zhao, M.: Seasonal and spatial variability of sea ice and phytoplankton biomarker flux in the Chukchi sea 495   (western Arctic Ocean), Prog. Oceanogr., 171, 22-37. https://doi.org/10.1016/j.pocean.2018.12.002, 2019.

Bai, Y., Sicre, M.-A., Ren, J., Jalali, B., Klein, V., Li, H., Lin, L., Ji, Z., Su, L., Zhu, Q., Jin, H. and Chen, J.: Centennial-scale variability of sea-ice cover in the Chukchi Sea since AD 1850 based on biomarker reconstruction, Environ. Res. Lett., 17, 4, https://doi.org/10.1088/1748-9326/ac5f92, 2022.

500   Bates, N.R. and Mathis, J.T.: The Arctic Ocean marine carbon cycle: evaluation of air-sea CO_2 exchanges, ocean acidification impacts and potential feedbacks. Biogeosciences, 6, 11, 2433-2459, https://doi.org/10.5194/bg-6-2433-2009, 2009.

Baskaran, M. and Naidu, A. S.: 210Pb-derived chronology and the fluxes of 210Pb and 137Cs isotopes into continental shelf sediments, East Chukchi Sea, Alaskan Arctic, Geochim. Cosmochim. Ac., 59, 505   4435–4448, https://doi.org/10.1016/0016-7037(95)00248-x, 1995.

Belt, S.T.: Source-specific biomarkers as proxies for Arctic and Antarctic sea ice, Org. Geochem., 125, 277-298, https://doi.org/10.1016/j.orggeochem.2018.10.002, 2018.

Belt, S.T.: What do IP_{25} and related biomarkers really reveal about sea ice change? Quat. Sci. Rev., 204, 216-219, https://doi.org/10.1016/j.quascirev.2018.11.025, 2019.

510   Belt, S.T., Brown, T.A., Rodriguez, A.N., Sanz, P.C., Tonkin, A. and Ingle, R.: A reproducible method for the extraction, identification and quantification of the Arctic sea ice proxy IP_{25} from marine sediments, Anal. Methods, 4(3), https://doi.org/ 10.1039/c2ay05728j, 2012.

Belt, S.T., Massé, G., Rowland, S.J., Poulin, M., Michel, C. and LeBlanc, B.: A novel chemical fossil of palaeo sea ice: IP_{25}, Org. Geochem., 38, 16-27, https://doi.org/10.1016/j.orggeochem.2006.09.013, 2007.

515   Belt, S.T., Massé, G., Vare, L.L., Rowland, S.J., Poulin, M., Sicre, M.-A., Sampei, M. and Fortier, L.: Distinctive ^{13}C isotopic signature distinguishes a novel sea ice biomarker in Arctic sediments and sediment traps, Mar. Chem., 112(3-4), 158-167, https://doi.org/10.1016/j.marchem.2008.09.002, 2008.

Belt, S.T., Smik, L., Brown, T.A., Kim, J.H., Rowland, S.J., Allen, C.S., Gal, J.K., Shin, K.H., Lee, J.I. and Taylor, K.W.: Source identification and distribution reveals the potential of the geochemical Antarctic sea ice proxy $IPSO_{25}$, Nat. Commun., 7, 12655, https://doi.org/10.1038/ncomms12655, 2016.

Bröder, L., Andersson, A., Tesi, T., Semiletov, I. and Gustafsson, Ö.: Quantifying Degradative Loss of Terrigenous Organic Carbon in Surface Sediments Across the Laptev and East Siberian Sea. Global Biogeochem. Cycles, 33, 85-99, https://doi.org/10.1029/2018GB005967, 2019.

Bröder, L., Tesi, T., Andersson, A., Eglinton, T. I., Semiletov, I . P., Dudarev, O. V., Roos, P., and Gustafsson, Ö.: Historical records of organic matter supply and degradation status in the East Siberian Sea, Org. Geochem., 91, 16–30, https://doi.org/10.1016/j.orggeochem.2015.10.008, 2016.

Brown, T.A. and Belt, S.T.: Biomarker-based H-Print quantifies the composition of mixed sympagic and pelagic algae consumed by *Artemia* sp, J. Exp. Mar. Biol. Ecol., 488, 32-37, https://doi.org/10.1016/j.jembe.2016.12.007, 2017.

Brown, T.A., Belt, S.T., Tatarek, A. and Mundy, C.J.: Source identification of the Arctic sea ice proxy IP_{25}. Nat. Commun., 5, 4197, https://doi.org/10.1038/ncomms5197, 2014a.

Brown, T.A., Yurkowski, D.J., Ferguson, S.H., Alexander, C. and Belt, S.T.: H-Print: a new chemical fingerprinting approach for distinguishing primary production sources in Arctic ecosystems.   Environ. Chem. Lett., 12(3), 387-392. https://doi.org/10.1007/s10311-014-0459-1, 2014b.

Cai, W.-J., Chen, L., Chen, B., Gao, Z., Lee, S.H., Chen, J., Pierrot, D., Sullivan, K., Wang, Y. and Hu, X.: Decrease in the CO_2 uptake capacity in an ice-free Arctic Ocean basin. Science, 329(5991), 556-559. https://doi.org/10.1126/science.1189338, 2010.

Cavalieri, D.J., Gloersen, P., Parkinson, C.L., Comiso, J.C. and Zwally, H.J.: Observed hemispheric asymmetry in global sea ice changes, Science, 278(5340), 1104-1106, https://doi.org/10.1126/science.278.5340.1104, 1997.

Cavalieri, D.J. and Parkinson, C.L.: Arctic sea ice variability and trends, 1979–2010, The Cryosphere, 6(4), 881-889, https://doi.org/10.5194/tc-6-881-2012, 2012.

Cavalieri, D.J., Parkinson, C.L., Gloersen, P. and Zwally, H.J.: Sea Ice Concentrations from Nimbus-7 SMMR and DMSP SSM/I-SSMIS Passive Microwave Data, Version 1., NASA National Snow and Ice Data Center Distributed Active Archive Center (Digital media, updated yearly), Boulder, Colorado USA, 1996.

Coachman, L.K. and Aagaard, K.: On the water exchange through Bering Strait, Limnol. Oceanogr., 11, 44-59, https://doi.org/10.4319/lo.1966.11.1.0044, 1966.

Cooper, L.W. and Grebmeier, J.M.: Deposition patterns on the Chukchi shelf using radionuclide inventories in relation to surface sediment characteristics, Deep Sea Res., Part II, 152, 48-66. https://doi.org/10.1016/j.dsr2.2018.01.009, 2018.

Coupel, P., Ruiz-Pino, D., Sicre, M.A., Chen, J.F., Lee, S.H., Schiffrine, N., Li, H.L. and Gascard, J.C.: The impact of freshening on phytoplankton production in the Pacific Arctic Ocean, Prog. Oceanogr., 131,

113-125, https://doi.org/ 10.1016/j.pocean.2014.12.003, 2015.

555   Cronin, T.M., Polyak, L., Reed, D., Kandiano, E.S., Marzen, R. and Council, E.: A 600-ka Arctic sea-ice record from Mendeleev Ridge based on ostracodes, Quat. Sci. Rev., 79, 157-167, https://doi.org/10.1016/j.quascirev.2012.12.010, 2013.

de Vernal, A., Gersonde, R., Goosse, H., Seidenkrantz, M.-S. and Wolff, E.W.: Sea ice in the paleoclimate system: the challenge of reconstructing sea ice from proxies – an introduction, Quat. Sci.

560   Rev., 79, 1-8, https://doi.org/10.1016/j.quascirev.2013.08.009, 2013.

Fernandes, M.-B. and Sicre, M.-A.: The importance of terrestrial organic carbon inputs on Kara Sea shelves as revealed by n-alkanes, OC and δ^{13}C values, Org. Geochem., 31, 363-374, https://doi.org/10.1016/S0146-6380(00)00006-1, 2000.

Fritz, M., Vonk, J.E. and Lantuit, H.: Collapsing Arctic coastlines, Nat. Clim. Change, 7(1), 6-7,

565   https://doi.org/10.1038/nclimate3188, 2017.

Gal, J.K., Ha, S.Y., Park, J., Shin, K.H., Kim, D., Kim, N.Y., Kang, S.H. and Yang, E.J.: Seasonal flux of ice‐related organic matter during under‐ice blooms in the western Arctic Ocean revealed by algal lipid biomarkers, J. Geophys. Res.: Oceans, 127(2), https://doi.org/10.1029/2021jc017914 2022.

Giles, K.A., Laxon, S.W., Ridout, A.L., Wingham, D.J. and Bacon, S.: Western Arctic Ocean freshwater

570   storage increased by wind-driven spin-up of the Beaufort Gyre. Nat. Geosci., 5(3), 194-197, https://doi.org/10.1038/ngeo1379, 2012.

Goñi, M.A., O'Connor, A.E., Kuzyk, Z.Z., Yunker, M.B., Gobeil, C. and Macdonald, R.W.: Distribution and sources of organic matter in surface marine sediments across the North American Arctic margin, J. Geophys. Res.: Oceans, 118(9), 4017-4035. https://doi.org/10.1002/jgrc.20286, 2013.

575   Grebmeier, J.M., Cooper, L.W., Feder, H.M. and Sirenko, B.I.: Ecosystem dynamics of the Pacific-influenced Northern Bering and Chukchi Seas in the Amerasian Arctic, Prog. Oceanogr., 71, 331-361. https://doi.org/10.1016/j.pocean.2006.10.001, 2006.

Grotheer, H., Meyer, V., Riedel, T., Pfalz, G., Mathieu, L., Hefter, J., Gentz, T., Lantuit, H., Mollenhauer, G. and Fritz, M.: Burial and Origin of Permafrost‐Derived Carbon in the Nearshore Zone of the

580   Southern Canadian Beaufort Sea, Geophys. Res. Lett., 47(3), https://doi.org/10.1029/2019gl085897, 2020.

He, J., Zhang, F., Lin, L., Ma, Y. and Chen, J.: Bacterioplankton and picophytoplankton abundance, biomass, and distribution in the Western Canada Basin during summer 2008, Deep Sea Res., Part II, 81-84, 36-45, https://doi.org/10.1016/j.dsr2.2012.08.018, 2012.

585   Holmes, R. M., McClelland, J. W., Peterson, B. J., Tank, S. E., Bulygina, E., Eglinton, T. I., Gordeev, V. V., Gurtovaya, T. Y., Raymond, P. A., Repeta, D. J., Staples, R., Striegl, R. G., Zhulidov, A. V. and Zimov, S. A.: Seasonal and Annual Fluxes of Nutrients and Organic Matter from Large Rivers to the Arctic Ocean and Surrounding Seas, Estuaries Coasts, 35(2), 369-382, https://doi.org/10.1007/s12237-011-9386-6, 2011.

590 Hu, L., Liu, Y., Xiao, X., Gong, X., Zou, J., Bai, Y., Gorbarenko, S., Fahl, K., Stein, R. and Shi, X.: Sedimentary records of bulk organic matter and lipid biomarkers in the Bering Sea: A centennial perspective of sea-ice variability and phytoplankton community, Mar. Geol., 429, https://doi.org/10.1016/j.margeo.2020.106308, 2020.

Hunt, G. L., Blanchard, A. L., Boveng, P., Dalpadado, P., Drinkwater, K. F., Eisner, L., Hopcroft, R. R.,
595 Kovacs, K. M., Norcross, B. L., Renaud, P., Reigstad, M., Renner, M., Skjoldal, H. R., Whitehouse, A. and Woodgate, R. A.: The Barents and Chukchi Seas: Comparison of two Arctic shelf ecosystems, J. Mar. Syst., 109-110, 43-68, https://doi.org/10.1016/j.jmarsys.2012.08.003, 2013.

Jakobsson, M.: Hypsometry and volume of the Arctic Ocean and its constituent seas, Geochem., Geophys., Geosyst., 3(5), 1-18, https://doi.org/10.1029/2001GC000302, 2002.

600 Ji, Z., Jin, H., Stein, R., Li, Z., Bai, Y., Li, H., Zhang, Y. and Chen, J.: Distribution and Sources of Organic Matter in Surface Sediments of the Northern Bering and Chukchi Seas by Using Bulk and Tetraether Proxies, J. Ocean Univ. China, 18(3), 563-572, https://doi.org/10.1007/s11802-019-3869-7, 2019.

Jia, R., Mu, X., Chen, M., Zhu, J., Wang, B., Li, X., Astakhov, A. S., Zheng, M. and Qiu, Y.: Sources of
605 particulate organic matter in the Chukchi and Siberian shelves: clues from carbon and nitrogen isotopes, Acta Oceanol. Sin., 39(9), 96-108, https://doi.org/10.1007/s13131-020-1650-9, 2020.

Kim, J. -H., Gal, J. -K., Jun, S. -Y., Smik, L., Kim, D., Belt, S. T., Park, K., Shin, K. -H. and Nam, S. -I.: Reconstructing spring sea ice concentration in the Chukchi Sea over recent centuries: insights into the application of the PIP_{25} index, Environ. Res. Lett., 14(12), 125004, https://doi.org/10.1088/1748-
610 9326/ab4b6e, 2019.

Koch, C. W., Cooper, L. W., Grebmeier, J. M., Lalande, C. and Brown, T. A.: Seasonal and latitudinal variations in sea ice algae deposition in the Northern Bering and Chukchi Seas determined by algal biomarkers, PLoS One, 15(4), e0231178, https://doi.org/10.1371/journal.pone.0231178, 2020.

Kolling, H. M., Stein, R., Fahl, K., Sadatzki, H., Vernal, A. and Xiao, X.: Biomarker Distributions in
615 (Sub)‐Arctic Surface Sediments and Their Potential for Sea Ice Reconstructions, Geochem., Geophys., Geosyst., 21(10), https://doi.org/10.1029/2019gc008629, 2020.

Lannuzel, D., Tedesco, L., van Leeuwe, M., Campbell, K., Flores, H., Delille, B., et al.: The future of Arctic sea-ice biogeochemistry and ice-associated ecosystems, Nat. Clim. Change, 10(11), 983-992, https://doi.org/10.1038/s41558-020-00940-4, 2020.

620 Li, L., Liu, Y., Wang, X., Hu, L., Yang, G., Wang, H., Bosin, A. A., Astakhov, A. S., and Shi, X.: Early diagenesis and accumulation of redox-sensitive elements in East Siberian Arctic Shelves, Mar. Geol., 429, 106309, https://doi.org/10.1016/j.margeo.2020.106309, 2020.

Massé, G., Rowland, S. J., Sicre, M. -A., Jacob, J., Jansen, E. and Belt, S. T.: Abrupt climate changes for Iceland during the last millennium: evidence from high resolution sea ice reconstructions, Earth Planet.
625 Sci. Lett., 269, 565-569, https://doi.org/10.1016/j.epsl.2008.03.017, 2008.

Müller, J., Massé, G., Stein, R. and Belt, S. T.: Variability of sea-ice conditions in the Fram Strait over

the past 30,000 years, Nat. Geosci., 2(11), 772, https://doi.org/10.1038/ngeo665, 2009.

Müller, J., Wagner, A., Fahl, K., Stein, R., Prange, M. and Lohmann, G.: Towards quantitative sea ice reconstructions in the northern North Atlantic: A combined biomarker and numerical modelling approach, Earth Planet. Sci. Lett., 306, 137-148, https://doi.org/10.1016/j.epsl.2011.04.011, 2011.

Nittrouer, C. A., DeMaster, D. J., McKee, B. A., Cutshall, N. H., Larsen, I. L.: The effect of sediment mixing on Pb-210 accumulation rates for the Washington continental shelf, Mar. Geol., 54(3-4), 201–221, https://doi.org/10.1016/0025-3227(84)90038-0, 1984.

Onodera, J., Watanabe, E., Itoh, M., Harada, N., Honda, M. C., Tengberg, A., Tanaka, Y. and Kikuchi, T.: Interannual Variation of Settling Particles Reflects Upper‐Ocean Circulation in the Southern Chukchi Borderland, 2010‐2014, J. Geophys. Res.: Oceans, 126(12), https://doi.org/10.1029/2021jc017431, 2021.

Ouyang, Z., Li, Y., Qi, D., Zhong, W., Murata, A., Nishino, S., Wu, Y., Jin, M., Kirchman, D., Chen, L. and Cai, W. J.: The Changing CO_2 Sink in the Western Arctic Ocean From 1994 to 2019, Global Biogeochem. Cycles, 36(1), https://doi.org/10.1029/2021gb007032, 2022.

Ovall, B., Pickart, R.S., Lin, P., Stabeno, P., Weingartner, T., Itoh, M., Kikuchi, T., Dobbins, E. and Bell, S.: Ice, wind, and water: Synoptic-scale controls of circulation in the Chukchi Sea, Prog. Oceanogr., 199, https://doi.org/10.1016/j.pocean.2021.102707, 2021.

Overeem, I., Anderson, R. S., Wobus, C. W., Clow, G. D., Urban, F. E., and Matell, N.: Sea ice loss enhances wave action at the Arctic coast, Geophys. Res. Lett., 38, https://doi.org/10.1029/2011GL048681, 2011.

Parkinson, C. L., Cavalieri, D. J., Gloersen, P., Zwally, H. J. and Comiso, J. C.: Arctic sea ice extents, areas, and trends, 1978–1996, J. Geophys. Res., 104(C9), 20837-20856, https://doi.org/10.1029/1999JC900082, 1999.

Parmentier, F. W., Christensen, T. R., Rysgaard, S., Bendtsen, J., Glud, R. N., Else, B., van Huissteden, J., Sachs, T., Vonk, J. E. and Sejr, M. K.: A synthesis of the arctic terrestrial and marine carbon cycles under pressure from a dwindling cryosphere, Ambio, 46(Suppl 1), 53-69, https://doi.org/10.1007/s13280-016-0872-8, 2017.

Polyak, L., Belt, S. T., Cabedo-Sanz, P., Yamamoto, M. and Park, Y. -H.: Holocene sea-ice conditions and circulation at the Chukchi-Alaskan margin, Arctic Ocean, inferred from biomarker proxies, The Holocene, 26(11), 1810-1821, https://doi.org/10.1177/0959683616645939, 2016.

Polyakov, I. V., Alekseev, G. V., Bekryaev, R. V., Bhatt, U. S., Colony, R., Johnson, M. A., Karklin, V. P., Walsh, D. and Yulin, A. V.: Long-term ice variability in Arctic marginal seas, J. Clim., 16(12), 2078-2085, https://doi.org/10.1175/1520-0442(2003)0162.0.CO;2, 2003.

Rantanen, M., Karpechko, A. Y., Lipponen, A., Nordling, K., Hyvärinen, O., Ruosteenoja, K., Vihma, T. and Laaksonen, A.: The Arctic has warmed nearly four times faster than the globe since 1979, Commun. Earth. Environ., 3(1), https://doi.org/10.1038/s43247-022-00498-3, 2022.

Rawlins, M. A., Connolly, C. T. and McClelland, J. W.: Modeling Terrestrial Dissolved Organic Carbon Loading to Western Arctic Rivers, J. Geophys. Res.: Biogeosci., https://doi.org/10.1029/2021jg006420, 2021.

Ren, J., Chen, J., Bai, Y., Sicre, M. -A., Yao, Z., Lin, L., Zhang, J., Li, H., Wu, B., Jin, H., Ji, Z., Zhuang, Y. and Li, Y.: Diatom composition and fluxes over the Northwind Ridge, western Arctic Ocean: Impacts of marine surface circulation and sea ice distribution, Prog. Oceanogr., 186, 102377, https://doi.org/10.1016/j.pocean.2020.102377, 2020.

Schubert, C. J. and Calvert, S. E.: Nitrogen and carbon isotopic composition of marine and terrestrial organic matter in Arctic Ocean sediments: implications for nutrient utilization and organic matter composition, Deep Sea Res., Part I, 48, 789-810, https://doi.org/10.1016/s0967-0637(00)00069-8, 2001.

Serreze, M. C. and Francis, J. A.: The Arctic Amplification Debate, Clim. Change, 76(3-4), 241-264, https://doi.org/10.1007/s10584-005-9017-y, 2006.

Serreze, M. C. and Stroeve, J.: Arctic sea ice trends, variability and implications for seasonal ice forecasting, Philos. Trans. R. Soc., A, 373, 20140159, https://doi.org/10.1098/rsta.2014.0159, 2015.

Shindell, D. and Faluvegi, G.: Climate response to regional radiative forcing during the twentieth century, Nat. Geosci., 2(4), 294, https://doi.org/10.1038/ngeo473, 2009.

Smik, L., Cabedo-Sanz, P. and Belt, S. T.: Semi-quantitative estimates of paleo Arctic sea ice concentration based on source-specific highly branched isoprenoid alkenes: a further development of the PIP_{25} index, Org. Geochem., 92, 63-69, https://doi.org/10.1016/j.orggeochem.2015.12.007, 2016.

Sparkes, R. B., Doğrul Selver, A., Bischoff, J., Talbot, H. M., Gustafsson, Ö., Semiletov, I. P., Dudarev, O. V. and van Dongen, B. E.: GDGT distributions on the East Siberian Arctic Shelf: implications for organic carbon export, burial and degradation, Biogeosciences, 12(12), 3753-3768, https://doi.org/10.5194/bg-12-3753-2015, 2015.

Stein, R., Fahl, K., Schade, I., Manerung, A., Wassmuth, S., Niessen, F. and Nam, S. -I.: Holocene variability in sea ice cover, primary production, and Pacific-Water inflow and climate change in the Chukchi and East Siberian Seas (Arctic Ocean), J. Quat. Sci., 32(3), 362-379, https://doi.org/10.1002/jqs.2929, 2017.

Stein, R., Macdonald, R. W., Naidu, A. S., Yunker, M. B., Gobeil, C., Cooper, L. W., Grebmeier, J. M., Whitledge, T. E., Hameedi, M. J., Petrova, V. I., Batova, G. I., Zinchenko, A. G., Kursheva, A. V., Narkevskiy, E. V., Fahl, K., Vetrov, A., Romankevich, E. A., Birgel, D., Schubert, C., Harvey, H. R. and Weiel, D.: The Organic Carbon Cycle in the Arctic Ocean, Stein, R. and MacDonald, R.W. (eds), pp. 169-314, Springer Berlin Heidelberg, Berlin, Heidelberg, 2004

Stoynova, V., Shanahan, T. M., Hughen, K. A. and de Vernal, A.: Insights into circum-Arctic sea ice variability from molecular geochemistry, Quat. Sci. Rev., 79, 63-73, https://doi.org/10.1016/j.quascirev.2012.10.006, 2013.

Stroeve, J., Holland, M. M., Meier, W., Scambos, T. and Serreze, M.: Arctic sea ice decline: faster than forecast, Geophys. Res. Lett., 34(9), https://doi.org/10.1029/2007gl029703, 2007.

700   Su, L., Ren, J., Sicre, M. A., Bai, Y., Jalali, B., Li, Z., Jin, H., Astakhov, A. S., Shi, X. and Chen, J.: HBIs and Sterols in Surface Sediments Across the East Siberian Sea: Implications for Palaeo Sea‑Ice Reconstructions, Geochem., Geophys., Geosyst., 23(2), https://doi.org/10.1029/2021gc009940, 2022

Tanski, G., Wagner, D., Knoblauch, C., Fritz, M., Sachs, T. and Lantuit, H.: Rapid CO_2 release from eroding permafrost in seawater, Geophys. Res. Lett., 46(20), 11244-11252,
705   https://doi.org/10.1029/2019gl084303, 2019.

Tesi, T., Semiletov, I., Hugelius, G., Dudarev, O., Kuhry, P. and Gustafsson, Ö.: Composition and fate of terrigenous organic matter along the Arctic land‑ocean continuum in East Siberia: Insights from biomarkers and carbon isotopes, Geochim. Cosmochim. Acta, 133, 235-256, https://doi.org/10.1016/j.gca.2014.02.045, 2014.

710   Tian, F., Pickart, R. S., Lin, P., Pacini, A., Moore, G. W. K., Stabeno, P., Weingartner, T., Itoh, M., Kikuchi, T., Dobbins, E., Bell, S., Woodgate, R. A., Danielson, S. L. and Wang, Z.: Mean and seasonal circulation of the eastern Chukchi Sea from moored timeseries in 2013–2014, J. Geophys. Res.: Oceans, 126(5), https://doi.org/10.1029/2020jc016863, 2021.

Timmermans M. L. and Toole J. M. : The Arctic Ocean's Beaufort Gyre, Ann. Rev. Mar. Sci., 15, 223-
715   248, https://doi.org/10.1146/annurev-marine-032122-012034, 2023.

Tortell, P. D., Mills, M. M., Payne, C. D., Maldonado, M. T., Chierici, M., Fransson, A., Alderkamp, A. C. and Arrigo, K. R.: Inorganic C utilization and C isotope fractionation by pelagic and sea ice algal assemblages along the Antarctic continental shelf, Mar. Ecol.: Prog. Ser., 483, 47-66, https://doi.org/10.3354/meps10279, 2013.

720   Volkman, J. K.: A review of sterol markers for marine and terrigenous organic matter, Org. Geochem., 9(2), 83-99, https://doi.org/10.1016/0146-6380(86)90089-6, 1986.

Vonk, J. E., Sánchez-García, L., Van Dongen, B., Alling, V., Kosmach, D., Charkin, A., Semiletov, I. P., Dudarev, O. V., Shakhova, N. and Roos, P.: Activation of old carbon by erosion of coastal and subsea permafrost in Arctic Siberia, Nature, 489, 137-140, https://doi.org/10.1038/nature11392, 2012.

725   Walsh, J. E., Fetterer, F., Scott stewart, J. and Chapman, W. L.: A database for depicting Arctic sea ice variations back to 1850, Geogr. Rev., 107(1), 89-107, https://doi.org/10.1111/j.1931-0846.2016.12195.x, 2017.

Wang, K., Zhang, H., Han, X. and Qiu, W.: Sources and burial fluxes of sedimentary organic carbon in the northern Bering Sea and the northern Chukchi Sea in response to global warming, Sci. Total Environ.,
730   679, 97-105, https://doi.org/10.1016/j.scitotenv.2019.04.374, 2019a.

Wang, X., Li, Z., Jin, H., Zheng, H. and Chen, J.: Sources and degradation of organic carbon in the surface sediments across the Chukchi Sea, insights from lignin phenols, Haiyang xuebao (in Chinese with English abstract), 39(10), 19-31, https://doi.org/10.3969/j.issn.0253-4193.2017.10.002, 2017.

Wang, Y., Bi, H., Huang, H., Liu, Y., Liu, Y., Liang, X., Fu, M. and Zhang, Z.: Satellite-observed trends
735   in the Arctic sea ice concentration for the period 1979–2016, J. Oceanol., Limnol., 37(1), 18-37, https://doi.org/CNKI:SUN:HYFW.0.2019-01-002, 2019b.

Watanabe, E., Onodera, J., Harada, N., Honda, M. C., Kimoto, K., Kikuchi, T., Nishino, S., Matsuno, K., Yamaguchi, A., Ishida, A. and Kishi, M. J.: Enhanced role of eddies in the Arctic marine biological pump, Nat. Commun., 5, 3950, https://doi.org/10.1038/ncomms4950, 2014.

740 Watanabe, E., Onodera, J., Itoh, M. and Mizobata, K.: Transport Processes of Seafloor Sediment From the Chukchi Shelf to the Western Arctic Basin, J. Geophys. Res.: Oceans, 127(4), https://doi.org/10.1029/2021jc017958, 2022.

Weingartner, T. J., Danielson, S., Sasaki, Y., Pavlov, V. and Kulakov, M.: The Siberian Coastal Current: A wind- and buoyancy-forced Arctic coastal current, J. Geophys. Res.: Oceans, 104(C12), 29697-29713, 745 https://doi.org/10.1029/1999jc900161, 1999.

Wheeler, P. A., Gosselin, M., Sherr, E., Thibault, D., Kirchman, D. L., Benner, R. and Whitledge, T. E.: Active cycling of organic carbon in the central Arctic Ocean, Nature, 380(6576), 697-699, https://doi.org/10.1038/380697a0, 1996.

Williford, K. H., Ward, P. D., Garrison, G. H. and Buick, R.: An extended organic carbon-isotope record 750 across the Triassic–Jurassic boundary in the Queen Charlotte Islands, British Columbia, Canada, Palaeogeogr., Palaeoclimatol., Palaeoecol., 244(1-4), 290-296, https://doi.org/10.1016/j.palaeo.2006.06.032, 2007.

Wild, B., Shakhova, N., Dudarev, O., Ruban, A., Kosmach, D., Tumskoy, V., Tesi, T., Grimm, H., Nybom, I., Matsubara, F., Alexanderson, H., Jakobsson, M., Mazurov, A., Semiletov, I. and Gustafsson, 755 O.: Organic matter composition and greenhouse gas production of thawing subsea permafrost in the Laptev Sea, Nat. Commun., 13(1), 5057, https://doi.org/10.1038/s41467-022-32696-0, 2022.

Woodgate, R., and Peralta‐Ferriz, C.: Warming and freshening of the Pacific inflow to the Arctic from 1990‐2019 implying dramatic shoaling in Pacific Winter Water ventilation of the Arctic water column, Geophys. Res. Lett., 48(9), https://doi.org/10.1029/2021gl092528, 2021.

760 Woodgate, R. A.: Increases in the Pacific inflow to the Arctic from 1990 to 2015, and insights into seasonal trends and driving mechanisms from year-round Bering Strait mooring data, Prog. Oceanogr., 160, 124-154, https://doi.org/10.1016/j.pocean.2017.12.007, 2018.

Woodgate, R. A., Aagaard, K. and Weingartner, T. J.: Monthly temperature, salinity, and transport variability of the Bering Strait through flow, Geophys. Res. Lett.,32, L04601, 765 https://doi.org/10.1029/2004gl021880, 2005.

Xiao, X., Fahl, K., Müller, J. and Stein, R.: Sea-ice distribution in the modern Arctic Ocean: Biomarker records from trans-Arctic Ocean surface sediments, Geochim. Cosmochim. Acta, 155, 16-29, https://doi.org/10.1016/j.gca.2015.01.029, 2015a.

Xiao, X., Fahl, K. and Stein, R.: Biomarker distributions in surface sediments from the Kara and Laptev 770 seas (Arctic Ocean): indicators for organic-carbon sources and sea-ice coverage, Quat. Sci. Rev., 79, 40-52, https://doi.org/10.1016/j.quascirev.2012.11.028, 2013.

Xiao, X., Stein, R. and Fahl, K.: MIS 3 to MIS 1 temporal and LGM spatial variability in Arctic Ocean sea ice cover: reconstruction from biomarkers, Paleoceanography, 30(7), 969-983,

https://doi.org/10.1002/2015PA002814, 2015b.

775 Zhang, R., Wang, H., Fu, Q., Rasch, P. J., Wu, M. and Maslowski, W.: Understanding the cold season Arctic surface warming trend in recent decades, Geophys. Res. Lett., 48(19), https://doi.org/10.1029/2021gl094878, 2021.

Zhuang, Y., Jin, H., Cai, W. J., Li, H., Qi, D. and Chen, J.: Extreme nitrate deficits in the western Arctic Ocean: Origin, decadal changes, and implications for denitrification on a polar marginal shelf, Global
780 Biogeochem. Cycles, https://doi.org/10.1029/2022gb007304, 2022.